Journal of Advanced Research 56 (2024) 69–86

Contents lists available at ScienceDirect

Journal of Advanced Research

journal homepage: www.elsevier.com/locate/jare

Original Article

ENOX2 inhibition enhances infiltration of effector memory *T*-cell and mediates response to chemotherapy in immune-quiescent nasopharyngeal carcinoma

Ngar-Woon Kam [a,b], Olivier Laczka [c], Xiang Li [c], John Wilkinson [c], Desmond Hung [a], Syrus Pak Hei Lai [a], Ka Chun Wu [a,b], Sai Wa Tsao [d], Wei Dai [a], Chi Ming Che [b,e], Victor Ho-Fun Lee [a,f], Dora Lai-Wan Kwong [a,f,*]

[a] *Department of Clinical Oncology, Li Ka Shing Faculty of Medicine, The University of Hong Kong, Hong Kong, China*
[b] *Laboratory of Synthetic Chemistry and Chemical Biology Limited, Hong Kong, China*
[c] *Noxopharm Limited, Level 20, Tower A, The Zenith, 821 Pacific Highway, CHATSWOOD NSW 2067, Australia*
[d] *School of Biomedical Sciences, Li Ka Shing Faculty of Medicine, The University of Hong Kong, Hong Kong, China*
[e] *Department of Chemistry, Faculty of Science, The University of Hong Kong, Hong Kong, China*
[f] *Clinical Oncology Center, The University of Hong Kong-Shenzhen Hospital, Shenzhen, China*

HIGHLIGHTS

- High ENOX2 expression is associated with immune excluded/deserted phenotypes in NPC.
- ENOX2 inhibitor, idronoxil enhances $CD8^+$ memory *T*-cell immunity in response to chemotherapy.
- Combined treatment with idronoxil and cisplatin enhances tumor response in humanized mice model.
- Combined treatment increases $CD8^+$ *T*-cell expansion with cytolytic effector memory (Tem) feature.
- *T*-cell infiltrates and tumor-associated ENOX2 have predictive value for anti-tumor response.

GRAPHICAL ABSTRACT

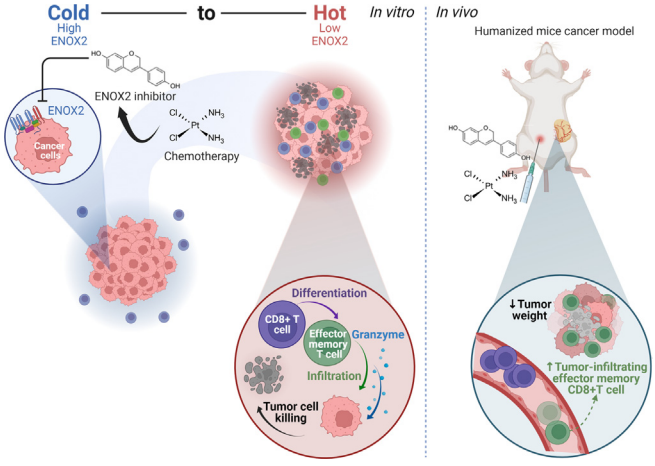

ARTICLE INFO

Article history:
Received 3 August 2022
Revised 1 February 2023
Accepted 1 April 2023
Available online 13 April 2023

Keywords:
Cisplatin
Cytotoxicity
Idronoxil
Memory *T*-cells

ABSTRACT

Introduction: The immunosuppressive tumor microenvironment is a major barrier for chemotherapy. Different chemosensitization approaches to reinstate immunological surveillance for cancers that are immune quiescent at the outset, have thus been devised. Cancer-specific ENOX2 expression is correlated with abnormal cell growth and has been proposed as a cellular target for anti-cancer activity. However, the potential effects of ENOX2 on the interaction between immune system and tumor cells remain elusive.

Objectives: To understand the mechanisms by which tumor-intrinsic ENOX2-mediated alterations in anti-tumor activity of *T*-cells and response to chemotherapy.

Methods: *In situ* multiplexed immunohistochemistry with single cell and bulk RNA sequencing data from nasopharyngeal carcinoma (NPC) human tissues were used to define tumor phenotypes. Two NPC cell

Peer review under responsibility of Cairo University.

* Corresponding author at: 1/F, Professorial Block, Queen Mary Hospital, 102 Pokfulam Road, Hong Kong, China.
E-mail address: dlwkwong@hku.hk (D.L.-W. Kwong).

https://doi.org/10.1016/j.jare.2023.04.001

ENOX2
Nasopharyngeal carcinoma

lines, with distinct ENOX2 expression, were used in a co-culture platform to study tumor-immune interactions between cancer cells/spheroids and *T*-cells. The effect of cisplatin treatment with ENOX2 inhibition by idronoxil (IDX) were tested *in vitro* and *in vivo*. Multi-parametric flow cytometry was used to characterize *T*-cell infiltrates in an NPC tumor humanized mouse model treated with combined treatment.

Results: NPC predominantly displayed an immune-excluded profile. This "cold-phenotype" was shown to exhibit higher ENOX2 expression and was associate with poorer progression-free survival (PFS). The therapeutic combination of IDX with cisplatin was effective in promoting $CD8^+$ effector memory T cell (Tem) differentiation and mobilization. This Tem signature was highly cytotoxic, with Tem-mediated preferential lysis of higher ENOX2-expressing NPC cells. A combination-treated humanized mouse model showing dramatic shrinkage in tumors, were intra-tumoral Tem-enriched.

Conclusion: Tumor-intrinsic ENOX2 expression is associated with tumor phenotype and PFS in NPC. Targeting ENOX2 with IDX and cisplatin impose qualitative control of *T*-cell response by preferentially increasing immune cells infiltration, Tem differentiation and tumor suppression. We suggest that ENOX2 inhibition may be a promising therapeutic strategy to enhance the effects of chemotherapy.

Introduction

Nasopharyngeal carcinoma (NPC), a cancer that frequently shows high sensitivity to radio- and chemotherapy, is endemic in Southern China, Southeast Asia, North Africa, and the Arctic, with undifferentiated, nonkeratinizing squamous cell carcinoma as the predominant histology [1]. While conventional chemotherapeutic drugs can impact rapidly dividing cancer cells, these agents can have toxic side effects, and tumor cells may develop resistance. This results in a 30–50 % relapse rate within 5 years after radical chemoradiotherapy [2], highlighting the urgent need to develop more durable treatment options for NPC.

Our team [3] and other research groups [4] have conducted previous studies on single-cell transcriptome analysis aimed at establishing the role of T cells in the pathogenesis of NPC. In those studies, *T*-cell subtype changes were detected in tumor tissue from patients with NPC, suggesting a transitional process whereby effector T cells gradually became less cytotoxic within the tumor microenvironment (TME). Protective immunity against cancer has previously been assigned to memory T cells, which are capable of durably persisting and functioning throughout host tissues and tumors, making them a gold standard for anti-tumor immunity. The T cell compartment can be subdivided according to their different cell surface marker expression and their effector functions. They comprise naive (Tn), central memory (Tcm), effector memory (Tem) and terminally differentiated (Temra) cells [5,6]. To date, *T*-cell types with memory properties have previously been reported to be superior in mediating anti-tumor responses, including: 1) lower activation thresholds than Tn cells, and 2) enhanced capacity to infiltrate/migrate and persist locally, providing immediate effector function at the site of tissue inflammation [7,8]. In various cancer types, numbers and activation states of immune effector cells, in particular, tumor-infiltrating T cells, have predictive value with respect to the anti-tumor response [9,10]. There are reasons to believe that certain cancer patients who are resistant to current therapeutic approaches may display a lack of *T*-cell immunity within the tumor nest, known as immunologically "cold tumors".

Ecto-NADH oxidase disulfide-thiol exchanger Type 2 (ENOX2), functions as a growth-related cancer-specific protein, is a tumor-associated cell surface ubiquinol (NADH) oxidase. To date, the molecular understanding of ENOX2 is mainly confined to the abnormal cell growth and division associated with the malignant phenotype [11]. Isoflavonoid derivatives, such as idronoxil (IDX), blocks the catalytic activity of ENOX2 [12] on cell growth or acts as a chemosensitizer in certain types of cancer [13]. While IDX's inhibitory effect on ENOX2 has been proposed to explain its cancer specificity, other authors have also reported that it may also target non-malignant proliferating lymphocytes [14] and stimulate natural killer cells [15]. Although these two studies support the view that IDX may not exclusively affect malignant cells, the extent to which these modes of action can be generalized remain unanswered. Moreover, no data are currently available that address the mechanisms by which IDX displays its bimodal action, as a chemosensitizer (via ENOX2) and as a modulator of immunological functions, including its interaction with the immune system within the TME.

The combination of IDX and radiotherapy have shown promising results for the treatment of patients with prostate cancer [16,17]. Another phase I trial showed that IDX can be combined with chemotherapy, carboplatin, and exerted anti-tumor activity in a boarder range of cancer patients [18]. However, it remains unclear whether the IDX has additional mechanisms in potentiating effects of radiotherapy or chemotherapy beyond ENOX2 inhibition. An important aspect is that current chemotherapeutic drugs can induce *T*-cell depletion [19,20] and impair their metabolism [21], thereby impacting both survival and functionality of different *T*-cell subsets [22]. With the lower cytotoxic *T*-cell immunity commonly displayed in NPC, therapeutic approaches which combine current standards of care with a drug that can potentiate the immune response has great appeal.

By combining *in situ* multiplexed immunohistochemistry with single cell and bulk RNA sequencing data from NPC human tissues, we demonstrated that NPC predominantly displays a "cold-phenotype", featuring a distribution of $CD8^+$ T cells in the tumor margin, with high ENOX2 expression in the tumor center. Furthermore, we have showed that $CD8^+$ memory *T*-cell based immune activities in the tumor can be enhanced with ENOX2 inhibition and combined treatment with chemotherapy, cisplatin (Cis), in both *in vitro* and *in vivo* NPC cancer models. While Cis alone showed limited *T*-cell-mediated lysis of NPC cells, the addition of IDX led to an enhanced cytotoxicity, preferentially against NPC cells expressing higher levels of ENOX2. These findings may have significant implications for the selection and the generation of optimal anti-tumor *T*-cell responses by targeting ENOX2 in cancer patients treated with chemotherapy and complicated by "cold" tumor phenotype.

Materials and methods

Cells, tissues and reagents

Three EBV + NPC cell lines (C17, C666, and NPC43), three EBV- NPC cell lines (NPC53, NPC38, and HK1) and two immortalized nasopharyngeal epithelial cell lines (NP460 and NP69) were kindly

provided by Professor George Tsao. C666-1 was cultured in RPMI-1640 medium (Invitrogen) supplemented with 10 % fetal bovine serum (FBS) and 1 % penicillin. NPC43, C17, NPC38, and NPC53 werecultured in RPMI-1640 medium supplemented with 10 % FBS, 1 % penicillin and 2 mM Y27632rock inhibitor (Enzo Life Sciences, ALX-270–333). NP460 were cultured in defined keratinocyte–serum-free medium and EpiLife (1:1) with supplements (Gibco, MEPI500CA), 10 % FBS and 1 % penicillin. NP69 was cultured in Keratinocyte SFM (Gibco, 10744019) supplemented with Bovine Pituitary Extract (BPE), 1 ng/ml epidermal growth factor (EGF), and 1 % penicillin. The HLA types of cell lines used for subsequent coculture assays are listed in Supplementary table 1 . NPC tissue samples used in this study were obtained from patients admitted to Queen Mary Hospital, the University of Hong Kong. Written informed consent was obtained from all participants. Tissues were fixed and subjected to histological examination. Tissue microarray (TMA) composed of samples from a total of 118 NPC patients from the Queen Mary Hospital, of those, 86 patients was used to evaluate *T*-cell spatial analysis and ENOX2 expression by multiplexed-IHC (32 cases were excluded due to deficit of data on cytokeratin-5 or insufficient sample material from TMA core). Peripheral blood mononuclear cells (PBMCs) were isolated from healthy donors (buffy coats, Hong Kong Red Cross Blood Transfusion Service) for subsequent culture. IDX (provided by Noxopharm Limited, Australia) was suspended in DMSO at 40 mg/mL (stock solution) and stored at –80 °C. Serial dilutions of the stock solution were freshly prepared in complete medium, used within 4 weeks, and stored at −20 °C. In all cultures, the final concentration of DMSO in the medium was ≤ 0.1 %.

PBMC separation and expansion of T cells

PBMCs were isolated from healthy donors by Ficoll-Paque gradient (GE Healthcare) and centrifuged at 400 × g for 25 min. The interface containing PBMCs was carefully removed and cells were washed twice with PBS + 2 mM EDTA, followed by cryopreservation in FBS/DMSO (90 %/10 %) for future analysis. Cryopreserved PBMCs were rapidly thawed and resuspended in RPMI1640 supplemented with 10 % heat-inactivated foetal bovine serum (FBS, Invitrogen), 1 % Hepes and 1 % Penicillin/Streptomycin (Gibco). On day 3, and every 3–4 days thereafter, the cultures were supplemented with the appropriate growth medium containing 120 IU/mL of recombinant IL-2 (Miltenyi biotec). On day 7, cells were phenotyped and enumerated using Multitest 6-Color TBNK Reagent (BD Biosciences) to ensure enrichment of $CD4^+$ and $CD8^+$ cells in the cultured cells, before subsequent co-culture studies. The antigen specificities and HLA restrictions of the PBMC products are shown in Supplementary table 2.

Colony formation and cell apoptosis assay

Colony formation was performed by culturing NPC cells (2×10^3 cells per well) in 6-well plates for 12 h before the indicated nominal concentrations of drugs were added. Cells were then fixed and stained using 1 % crystal violet. For the apoptosis assay, the apoptotic cells were quantified (percentage) using an Annexin V-FITC/propidium iodide (PI) apoptosis detection kit (BD Biosciences). See details under Supplementary Method.

Cell viability assay

Cells (3×10^3 cells per well) were cultured in 96-well plates containing 200 μL of culture medium for 12 h. Following cell adhesion, indicated compounds were added at eight different concentrations, using a threefold serial dilution and a maximum concentration of 40 μM, for 72 h. Following culture, the cell proliferation kit reagent (XTT; Roche) was added to the culture wells and incubated for 4 h at 37 °C. The absorbance value was measured using a spectrophotometer at 450 nm. All treatments were performed in triplicate and each experiment was conducted at least three times. Nonlinear regression was used to determine the half-maximal inhibitory concentration (IC_{50}) values and dose–response curves. IC_{50} was read from the viability curve at the point of 50 % viability and according to the formula %viability = (Reading-positive control)/ (DMSO-positive control) x100. Proteasome at 10 μM was used as a positive control. Moreover, drug-combination effects were analyzed using the R package SynergyFinder Version 1.6.1 to calculate the Zero Interaction Potency (ZIP) score for each concentration tested, whereby CI values < -10, −10 to 10, and > 10 indicated antagonism, additivity and synergy, respectively.

Co-culture and multi-parametric flow cytometry

C17 and NPC43 NPC cell lines were pre-treated with indicated doses of IDX and/or Cis for 24 h before coculturing with PBMCs *via trans*-wells (3 μm pore-size, Corning) for 3 days. For phenotypic surface staining, PBMCs were collected, washed and resuspended in FACS buffer (PBS, 0.5 % BSA and 2 mM EDTA). Cells were pre-treated with Fc block reagents (1:200; Biolegend), then stained with a mix of surface fluorophore-conjugated anti-mouse antibodies: CD8-APCH7, CD4-BV421, CD45RA-PECy5, CD62L-BV605. $CD4^+$ and $CD8^+$ *T*-cell subsets were first gated and then defined as: T naïve (Tn): $CD45RA^+CD62L^+$; T central-memory (Tcm): $CD45RA^-CD62L^+$; T effector-memory (Tem) $CD45RA^-CD62L^-$; T effector-memory re-expressing CD45RA (Temra): $CD45RA^+CD62L^-$. For details on antibodies and staining procedures, see Supplementary Method and Supplementary table 3.

Chemotaxis assay

Directional migration of PBMCs was evaluated in Costar Transwell permeable polycarbonate supports (5-μm pores) in 24-well plates. Briefly, drug-treated/untreated tumor cells were pre-plated and stimulated for 3 days while PBMCs were co-stimulated using anti-CD3/anti-CD28 (Miltenyi Biotec) for one days. After that, the primed PBMCs prepared at a density of 0.25×10^6 cells/ml serum-free RPMI 1640 medium were placed in the upper chamber. The plate was then incubated in a 37 °C cell culture incubator for 5 h. The cells present in the bottom chambers were collected, stained with antibodies against CD45, CD3, CD4, CD8, CD45RA and CD62L, and the number of migrated cells was calculated by flow cytometry. For details on antibodies and staining procedures, see Supplementary Method and Supplementary table 3.

Cytotoxicity assay

NPC cell lines were labeled with 5 μM CFSE (Sigma, catalog 21888), seeded in a 96-well plate at 10^5 cells/well, and T cells previously co-cultured with drug-treated tumor cells (generated as above) were added at the indicated ratios and cultured for 72 h. Cells were stained with Fixable Viability Dye eFluor 780 (BD Biosciences), and staining was evaluated by flow cytometry as previously described. The percentage of specific lysis was then calculated using the following equation: % specific lysis = 100 × (% specific cell death - % basal cell death)/100 - % basal cell death. Specific cell death was determined from viability dye staining of CFSE-positive cells in the *T*-cell co-culture wells, and basal cell death from wells lacking co-cultured T cells.

Mitochondrial membrane potential (ΔΨm) analysis

JC-1 was used to investigate changes in mitochondrial membrane potential (ΔΨm), according to previous studies. For details analysis procedures, see Supplementary Method.

Western blot

Cells were lysed in RIPA buffer containing protease and phosphatase inhibitors on ice for 45 min and collected by centrifuging at 150,000 rpm for 15 min at 4 °C. Protein concentrations were measured by the bicinchoninic acid protein assay kit (Pierce). Equal amounts of protein were solubilized in laemmili buffer, boiled for 5 min and then separated by 10 % SDS-PAGE before transferring onto nitrocellulose membranes. Membranes were blocked and probed with primary antibodies (Supplementary table 4), detected using appropriate HRP-conjugated secondary antibodies and visualized by incubation with enhanced chemiluminescence reagent (ECL, GE Healthcare) and exposure to film.

Cytokine and antibody arrays

Human Inflammation Antibody Array C3 (RayBiotech) was used to detect cytokines and cell-factors in conditioned media from cells under indicated conditions. Cells were cultured in 6-well plates and treated with IDX, Cis or a combination of both. Culture medium was centrifuged 72 h later and evaluated using the human cytokine array according to the manufacturer's guidelines.

Quantitative real-time PCR (q-RTPCR)

Total RNA (500 ng) was extracted using an RNeasy mini kit (Qiagen) according to the manufacturer's instructions. Total RNA (500 ng) was reversed transcribed with Primescript RT (Takara), with the cDNA serving as the template for amplification. Quantitative real-time PCR was subsequently performed using SYBR Green Master Mix (Takara) on a LightCycler480 (Roche). Relative quantification was measured using the Comparative Ct (Threshold Cycle) with the Ct values normalized to GAPDH. All samples were analyzed in duplicate and the mean of the 2 runs was reported. Primers used are shown in Supplementary table 5.

Multiplex immunohistochemistry

Tyramide signal amplification (TSA) IHC staining was applied to the TMA slides. Slides were first deparaffinized and rehydrated in serial passages through xylene and alcohol. Heat-induced antigen retrieval was performed using a microwave. The sections on each slide were incubated with blocking solution, supplemented with 2 % BSA, for 15 min at room temperature (RT). Slides were incubated with primary antibodies: CD8 (Dako), ENOX2 (Abcam) and pan-cytokeratin-5 (PK; 1:50, DAKO) for 1 h at RT. Multiplexed TSA was visualized using a triplex (CD8 in Opal 570, PK in Opal 540, and ENOX2 in Opal 620). Slides were counterstained with DAPI for 5 min and mounted with VECTASHIELD. TMA sections were digitally scanned as previously described [23]. For details analysis procedures, see Supplementary Method.

Spheroid-infiltrating cells flow cytometry staining

For the generation of tumor spheroids in 3D, 200 µL/well of cell suspension in culture medium was seeded at cell densities of 20,000 cells/well. PBMCs (HLA-matched if possible) pre-stimulated with IL-2 were added 3 days after spheroid formation at the ratio of 10:1. On the day of co-culture, PBMCs were stained with MERCK Red Stain PKH26, following manufacturer instructions (Thermofisher), and spheroids were stained with 0.1 uM Invitrogen Cell Event, followed by drug administration. For details analysis procedures, see Supplementary Method. For flow cytometry analyses, 8 wells/condition were seeded. Immune cells that were either 'OUT', or 'IN' the spheroids, were compartmentalized by pooling the 8 co-culture wells in Eppendorf tubes. Spheroids were gently resuspended and left to sediment to the bottom of the tubes. The cell suspension, constituting non-infiltrating immune cells (=OUT), was removed and PBS was added twice in order to fully separate the spheroids from the non-infiltrating immune cells. Spheroids were then trypsinized to obtain a single cell suspension (=IN) and analyzed by flow cytometry.

Single cell RNA sequencing (scRNA -Seq) and transcriptomic expression analysis

The raw and processed single-cell sequencing data are publicly available in Gene Expression Omnibus (GEO) with the accession number GSE150825 and GSE162025.The publicly available NPC bulk RNA sequencing data used were downloaded from GEO with the accession number GSE34573, GSE53819 and GSE12452. The publicly available microarray data used were downloaded from GSE12452, GSE34573 and GSE64634. For details analysis procedures, see Supplementary Method.

In vivo tumor experiments

For drug response in tumorigenesis, thirty 8-week-old female nude mice per group were inoculated once subcutaneously, with 5×10^6 NPC cell lines + matrigel (1:1) using a 29-gauge needle under anaesthesia followed by indicated drug treatment. For drug responses in humanized mice, a model was established and performed by TransCure bioServices SAS (Archamps, France) using the female NOD-Prkdscid-IL-2rgTm1/Rj (NXG) immunodeficient mouse strain. Mice were humanized using hematopoietic stem cells ($CD34^+$) isolated from human cord blood. A total of 20 mice with > 25 % humanization rate (circulating human $CD45^+$, $hCD45^+$; $hCD45^+$/total $CD45^+$) were used in the study. For details analysis procedures, see Supplementary Method.

Statistics

Statistical analysis was performed with GraphPad Prism8 software. Unless indicated otherwise, data are expressed as mean ± standard error of the mean (SEM). Differences in quantitative variables were analyzed by the Mann–Whitney *U* test or unpaired Student's *t*-test when comparing variables between two groups. Kruskal–Wallis–ANOVA was performed to compare variables between three or more groups. The correlation was evaluated *via* Spearman's rank correlation coefficient. Survival outcomes were compared using the Kaplan–Meier method and the log-rank test. P values < 0.05 were considered statistically significant.

Ethics statement

The study was approved by the Institutional Review Board of The University of Hong Kong/Hospital Authority Hong Kong West Cluster (HKU/HA HKW IRB, UW16-428). All experiments involving animals were conducted according to the ethical policies and procedures approved by the Committee on the Use of Live Animals in Teaching and Research (CULATR) of the University of Hong Kong (protocol 5026–19).

Results

Clustering of immune cells by location identifies high ENOX2-expressing immune cold topography as a major NPC cancer hallmark

Within the TME, spatial distribution distinguishing between tumor region (pan-cytokeratin; PK + area; hereafter referred as T) and tumor stroma (PK-area; hereafter referred as S) is one of the important determinants for immune cell function. We previously reported [23] that spatial organization in the tumor architecture can provide more precise biological information compared to total cell densities alone. Based on this and other studies demonstrated the existence of "hot-tumors" and "cold-tumors" ("immune-deserted" and "immune-excluded" tumors), which was related to the level of cytotoxic immune cells infiltration [24,25], we here evaluated our dataset to gather evidence of this clustering and categorized NPC into three main groups (Fig. 1A-B). We used the median cell densities for $CD8^+$ cells as a cut-off value [>512 cells/mm^2 for CD8 counts in *T*-area to classify as "hot" phenotypes and < 512 cells/mm^2 as "cold" phenotypes; >788 cells/mm^2 for CD8 counts in S-area to classify "cold" tumors as either "immune-excluded" (tumors with only immune cells aggregating at the boundaries) and < 788 cells/mm^2 as "immune-deserted" (absence of immune cells)] to define spatial compartments in a tissue microarray (TMA) from 86 tumor formalin-fixed paraffin-embedded (FFPE) NPC tissues. In 59 tumors (68.6 %; with the cell density of $CD8^+$ was below median) were categorized as "cold-phenotypes", while 27 tumors (31.4 %; with $CD8^+$ cell densities above median) were categorized as "hot-phenotypes" (Fig. 1C; Supplementary Fig. 1A). As compared to the "cold" tumor, significantly higher densities of CD8 cells were expressed within the T area (hereafter referred as $CD8^+$ tumor-infiltrating lymphocytes (TIL-CD8), the S area (hereafter referred as $CD8^+$ nontumor-infiltrating lymphocytes (nonTIL-CD8; Fig. 1D), and the whole area (Supplementary Fig. 1B) was observed in the "hot" tumors. Moreover, we found that surface-based ENOX2 expression in reference to PK-expressing tumoral cells (PK^+ENOX2^+; hereafter referred as T ENOX2) was strongly represented in this cancer type (Fig. 1E). Moreover, such cancer-specific ENOX2 was expressed in higher densities as compared to the S area, and this feature correlated with lower counts of TIL-CD8 (Fig. 1F). More importantly, it was observed that the ENOX2 had a wide range of protein expression in the tumor within this cohort (Fig. 1G). Using the mean T ENOX2 expression in the cohort as a threshold of positivity, 50 % of individuals were defined as $ENOX2^+$. We selected tumors with the highest 20 % of ENOX2 expression ($ENOX2^{hi}$) and compared them with the group with the lowest 20 % of ENOX2 expression (($ENOX2^{lo}$). A higher percentage (66.7 %) of $ENOX2^{hi}$ group demonstrated a "cold tumor" phenotype, whereas 44.4 % of the $ENOX2^{lo}$ group were associated with a "hot" phenotype (Supplementary Fig. 1C). Similarly, T ENOX2 tended to be negatively correlated with TIL-CD8 in the $ENOX2^{hi}$ group (r = -0.43; Spearman correlation; p = 0.086), whereas a positive association was found within the $ENOX2^{lo}$ group (r = 0.44; Spearman correlation; p = 0.069) (Fig. 1H). In contrast with the described higher T ENOX2 negatively correlated with TIL-CD8, the association between TIL-CD8 densities and ENOX2-expressed malignant cells was lost in tissue mass (Supplementary Fig. 1D), highlighting the importance of delineating the spatial location of ENOX2 expression as well as of CD8 T cells to better understand how the TME architecture influences outcomes in NPC.

Examination of the ENOX2 prognostics value in a publicly available online survival database (GSE102349; n = 88) showed that NPC patients with higher levels of ENOX2 expression had a poorer progression-free survival (PFS) (PFS at 36 months for patients with ENOX2 low-, moderate- and high-group was 95 %, 79.7 %, and 54.9 %, respectively; Hazard Ratio (HR) = 4.94, 95 % confidence interval = 0.032; Fig. 1I). Meanwhile, ENOX2 was found to be highly expressed in NPC patients as compared to healthy individuals (Supplementary Fig. 1E-F) from public microarrays and RNA-Sequencing datasets (GSE12452, GSE34573, GSE53818 and GSE64634). We concluded that the TME of NPC patients largely exhibited a "cold" phenotype, that was commonly associated with high tumor ENOX2 expression and associated with poorer PFS.

Chemotherapy and IDX exhibits growth inhibitory effects, with varying susceptibility in three analyzed ENOX2-expressing NPC cell lines

As we found that the ENOX2 expression levels was associated with the severity of NPC cancer, IDX, an ENOX2 inhibitor, may thus provide a potential therapeutic benefit through its interaction with this target. We first identified that higher expression levels of ENOX2 were observed in Epstein-Barr virus (EBV)-positive tumor cells as compared to immortalized nasopharyngeal epithelial and EBV-negative tumor cells (Supplementary Fig. 2A). NPC is consistently associated with EBV infection, highlighting the therapeutic potential of IDX toward this cancer type.

Among the limited available authentic EBV-positive tumor cells, ENOX2 expression varied, such that NPC43, C666 and C17 showed highest to lowest levels of ENOX2 expression respectively (Supplementary Fig. 2B). Accordingly, IDX monotherapy exhibited anti-proliferative activity, as measured by the XTT assay, with 50 % inhibitory concentration (IC_{50}) values of 2.138, 2.036, 2.369 μM for NPC43, C17 and C666, respectively (Supplementary Fig. 3A). Based on these initial data, a target range for IDX (average dose ± 2-fold dilutions; 1, 2 and 4 μM) was selected to determine its anti-cancer effect through the induction of apoptosis. Annexin-V/PI assays revealed a dose-dependent increase in late-stage apoptotic cells after treatment with IDX when compared to the untreated control (Supplementary Fig. 3B). As expected, significance was reached for both NPC43 and C666, with the higher levels of ENOX2.

Further analysis on the treatment with Cis on the NPC43, C17 and C666, determined IC_{50} values of 1.760, 2.090, 3.305 μM, respectively (Supplementary Fig. 3C). A target range for Cis (2-to-4-fold dilutions of average dose; 0.6, 1.2, 2.4 μM) was selected. We then asked if IDX mediated the tumor killing effect of the Cis treatment, and if so, whether a treatment targeting ENOX2 would synergize with Cis and lead to a durable tumor response. While IDX or Cis monotherapy resulted in moderate suppression, their combination reduced the number of colonies formed to a significantly greater extent (Supplementary Fig. 3D). We further evaluated the anti-proliferative activity of the IDX/Cis combination and confirmed that IDX plus Cis suppressed NPC cell growth in a more potent and durable manner compared with either drug alone in a dose-dependent manner (Supplementary Fig. 3E). On that basis, the appropriate concentrations of Cis at 1.2 μM (thereafter referred as Cis1.2) and IDX at 2 μM (thereafter referred as IDX2) were selected for subsequent *in vitro* experiments. Notably, the extent of cell survival varied, with tumor cells showing higher expression of ENOX2 being more prone to the drug inhibition (∼2.5-, ∼3- and ∼ 9-fold decreased in viability for C17, C666 and NPC43, respectively). These results prompted us to hypothesize that combining IDX with Cis may impede tumor growth in a manner that is dependent on the amount of ENOX2 expressed. Moreover, the Zero interaction potency (ZIP) model, which was used to evaluate synergistic indexes, indicating potent additivity (ZIP score < 10), rather than synergy, between the activities of IDX and Cis against cancer cell proliferation (Supplementary Fig. 3F).

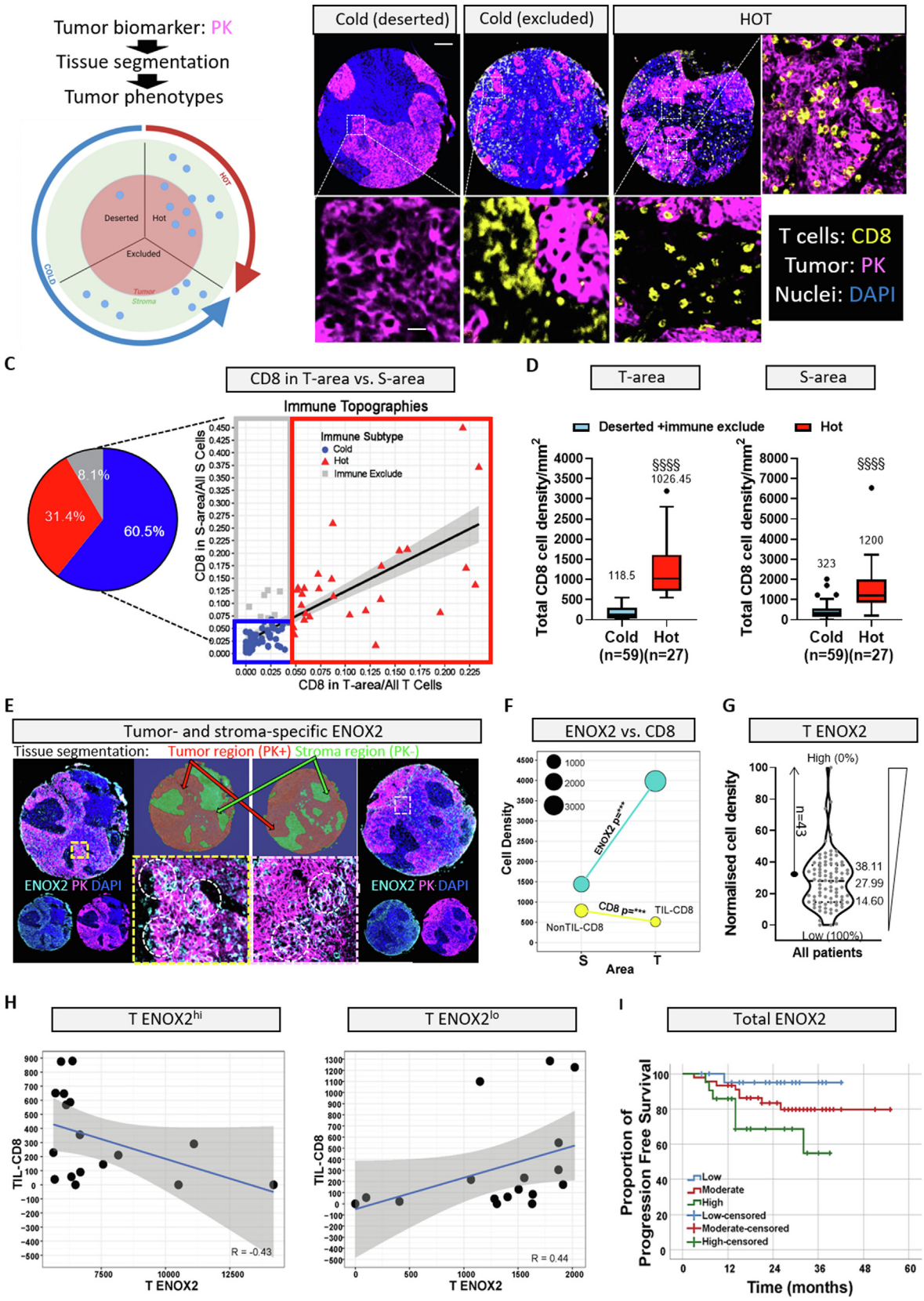
Tumor biomarker: PK
Tissue segmentation
Tumor phenotypes
Deserted
Hot
Excluded
HOT
COLD
Tumor
Stroma
Cold (deserted)
Cold (excluded)
HOT
T cells: CD8
Tumor: PK
Nuclei: DAPI
C
CD8 in T-area vs. S-area
Immune Topographies
8.1%
31.4%
60.5%
Immune Subtype
Cold
Hot
Immune Exclude
CD8 in S-area/All S Cells
CD8 in T-area/All T Cells
D
T-area
S-area
Deserted +immune exclude
Hot
Total CD8 cell density/mm2
§§§§
1026.45
118.5
323
1200
Cold
Hot
(n=59)(n=27)
E
Tumor- and stroma-specific ENOX2
Tissue segmentation:
Tumor region (PK+)
Stroma region (PK-)
ENOX2 PK DAPI
F
ENOX2 vs. CD8
Cell Density
ENOX2 p=***
CD8 p=***
TIL-CD8
NonTIL-CD8
S
T
Area
G
T ENOX2
High (0%)
Low (100%)
n=43
38.11
27.99
14.60
Normalised cell density
All patients
H
T ENOX2hi
T ENOX2lo
TIL-CD8
T ENOX2
R = -0.43
R = 0.44
I
Total ENOX2
Proportion of Progression Free Survival
Low
Moderate
High
Low-censored
Moderate-censored
High-censored
Time (months)

Inflammatory signatures are upregulated after combination therapy and may drive CD8 + T cell expansion and migration

The above-mentioned data showed that ENOX2 patterns were closely associated with specific histologic immune phenotypes of NPC. The extended distribution frequency of ENOX2 protein levels is undoubtedly due to heterogeneity between patients. We thus used two cell lines with distinct ENOX2 expression levels (C17 and NPC43, expressing relatively lower and higher levels of ENOX2, respectively) to better represent for the breadth of patients displaying different histologic features (C17 resembles histologically ENOX2^{lo} NPC and NPC43 resembles histologically ENOX2^{hi} NPC).

Forty different inflammatory factors in response to single agent (IDX or Cis) or in combination were evaluated in NPC43 *via* human antibody array analyses (Fig. 2A and Supplementary Fig. 4A). No major changes were identified in response to Cis treatment, whereas several inflammatory factors were markedly elevated upon IDX, or combination treatment, with TNFRSF1A displaying the highest magnitude in those upregulated proteins. qRT-PCR confirmed the protein array results and revealed an upregulated *TNFRSF1A* gene expression in NPC43, to a lesser extent in C17, upon combined Cis and IDX treatment (Supplementary Fig. 4B). Using the scRNA-Seq data of NPC tissues (GSE150430), we estimated TNFR-dependent *T*-cell functions in NPC. A significant difference was observed in TNFRSF1A-expressing tumor cells between low (TNFRSF1A^{lo}) and high (TNFRSF1A^{hi}) groups (dichotomized by a median cut-off (median 0.27 (TNFRSF1A^{lo}) vs 0.56 (TNFRSF1A^{hi})). To determine whether TNFRSF1A^{lo}-tumor cells reflected reduced TNF-TNFRSF1A interaction in NPC TME, we assessed the total amount of TNFα in T cells. We observed a significant difference in TNFα levels in pan-T cells between TNFRSF1A^{lo} and TNFRSF1A^{hi} groups, with similar trends observed in CD4/CD8 T cells (Fig. 2B). Prominent TNF-TNFRSF1A interaction in NPC tumors was observed, where there was higher tumor expression of TNFRSF1A, and this was associated with a higher TNFα-producing CD8$^+$ *T*-cell phenotype (Fig. 2C-D). To understand the interactions between cancer cells and tumor-infiltrating T cells in NPC, we used CellPhoneDB to predict the ligand-receptor interactions. Several known ligand-receptor pairs were identified to be differentially overexpressed in NPC (Supplementary Fig. 4C). Interestingly, apart from CXCL10, those chemokines/cytokines significantly induced by combined Cis and IDX treatment in tumor cells (the outgoing signals) showed weak interaction with different tumor infiltrating *T*-cell subsets (Supplementary Fig. 4D). This finding brings us to hypothesize that the combination therapy could provide a distinct pro-inflammatory milieu to boost *T*-cell immunity, potentially converting "cold" tumors into "hot". This potential mechanism was further supported by an enrichment of TNFα and TNFRSF1A levels in CD8 high/ "hot" tumors (dichotomized by a median cut-off; Fig. 2E). Therefore, we investigated whether the combination treatment could mediate immune activation within the TME of NPC. *In vitro* co-cultures of tumor cells with PBMCs (allogenic HLA-matched where possible) from healthy donors, at the selected drug doses, which demonstrated limited toxicity against PBMCs (Supplementary Fig. 5A), suggested that IDX and Cis did not affect immune viability individually. We utilized *t*-distributed stochastic neighbor embedding (*t*-SNE) to identify changes in cell populations after treatment from pooled co-cultures (C17 and NPC43). Based on major markers associated with immune cell lineages (CD4 for T helper cells; CD8 for T cytotoxic cells; CD14 for monocytes; CD19 for B cells and CD56 NK cells), Cis treatment group showed a similar *t*-SNE pattern to the control group treated with DMSO alone (Fig. 2F). By contrast, a new subset of CD8$^+$ T cells appeared after treatment with IDX alone or in combination with Cis. We further confirmed an increased CD8/CD4 ratio in the combined drug treatment group (NPC43 co-cultures, Fig. 2G; C17 co-cultures, Supplementary Fig. 5B), indicating that IDX enhanced the immunomodulatory effect of Cis on *T*-cell lineages. Transwell migration experiments were used to evaluate the effect of IDX combined with Cis on cell chemotaxis. Compared to the control group, IDX and Cis alone upregulated the migration of *T*-cell lineages. However, when combined, IDX and Cis significantly increased the migration of *T*-cell lineages, compared to the single drug treated groups, resulting in a marked synergistic effect on CD8$^+$ migration. This tendency reached significance when PBMCs were co-cultured in transwell with NPC43 (Fig. 2H) and was lost in C17 co-cultures (Supplementary Fig. 5C). These results suggest that the combined treatment may preferentially enhance immunostimulatory response to tumor cells with higher ENOX2 expression.

Combination therapy leads to a more efficient expansion of CD8$^+$ T cells exhibiting memory cell phenotypes in tumor cells with high ENOX2 expression

CD8$^+$ T cells are often considered to play an important role in tumor clearance, and memory CD8$^+$ *T*-cell induction in the context of cancer has been previously described [26,27]. We evaluated differential regulation processes of *T*-cell populations following drug

Fig. 1. Phenotyping of immune cell density-based subgrouping enables the evaluation of immune heterogeneity in NPC with ENOX2 expression. **(A)** Classification of tumor-immune phenotypes based on cell location in the tumor core and in the outer stromal area. **(B)** Representative three-plex multispectral IHC images for CD8 (yellow), pan-keratin (PK; pink) and DAPI (blue) depict the immune landscape in NPC with intra-tumor and *peri*-tumor areas with three distinct immune infiltration status ("deserted-cold", "excluded-cold" and "hot"). Three-color overlay (top three left) and enlarged insets with representative region of select combinations of markers (CD8 and PK) are shown on the side. Scale bar: 100 μm. **(C)** Linear regression of CD8$^+$ lymphocyte proportions in the area of tumor (T) and stroma (S) (plot) and correlation with three distinct immune landscapes ("deserted-cold", blue; "excluded-cold", grey; "hot", red) was shown. CD8 in *T*-area/all T cells = CD8$^+$ cell counts in tumor area/all tumor cells; CD8 in S-area/all S cells = CD8$^+$ cell counts in stromal area/all stromal cells. **(D)** The density of CD8$^+$ T cells as counts/mm^2 in the area of tumor (*T*-area) and stromal (S-area) of 59 cold (deserted-cold plus excluded-cold) and 27 "hot" tumors of NPC. **(E)** Representative multispectral of tissue segmentation (tumor regions in red, denoted as PK+; stromal regions in green, denoted as PK-) and IHC images for ENOX2 (turquoise) and PK (pink). Magnified insets with representative region (yellow broken lines) of select combinations of markers. White circle broken line shows co-staining of ENOX2 and PK. Scale bar: 100 μm. **(F)** The cell density of CD8$^+$ T cells as counts/mm^2 and ENOX expression in stroma (S; designated as "nontumor-infiltrating, nonTIL-CD8") and tumor (T; designated as tumor-infiltrating, TIL-CD8) areas. **(G)** Distribution of ENOX2 expression on tumor cells (T ENOX2) in the sampling cohort (n = 86). Equal number of cells per patient were selected to normalize between tumor cells. 50 % of the cohort was defined as ENOX2$^+$ with the mean expression (28.06 cell density/mm^2, n = 34) of the cohort. **(H)** Correlation between CD8 in the tumor area (T CD8) and tumor ENOX2 (T ENOX2) in high (ENOX2^{hi}; top 20 %) and low (ENOX2^{lo}; bottom 20 %) ENOX2 expression groups (n = 17, respectively). **(I)** Kaplan–Meier visualization of progress-free survival from diagnosis by ENOX2 expression. ENOX2 as low (1st quartile; blue), moderate (2nd and 3rd quartiles; red) and high (4th quartile; green) expressions. Data information: Data points are shown ± SEM. In the boxplots in (D, G), the centerline indicates the median, while the upper and lower lines represent the 75th and 25th percentiles, respectively. The whiskers represent the smallest and largest values in the 1.5 × interquartile range. Values on top indicate median. In (C, H), statistical evaluations were performed using Spearman's rank correlation test. In (D, F), P values were calculated with unpaired Mann–Whitney. In (I), Kaplan–Meier were analyzed using two-tailed log-rank test. §§§§p < 0.0001 compared to Deserted + immune excluded. ***p < 0.001 compared to cell density in S area.

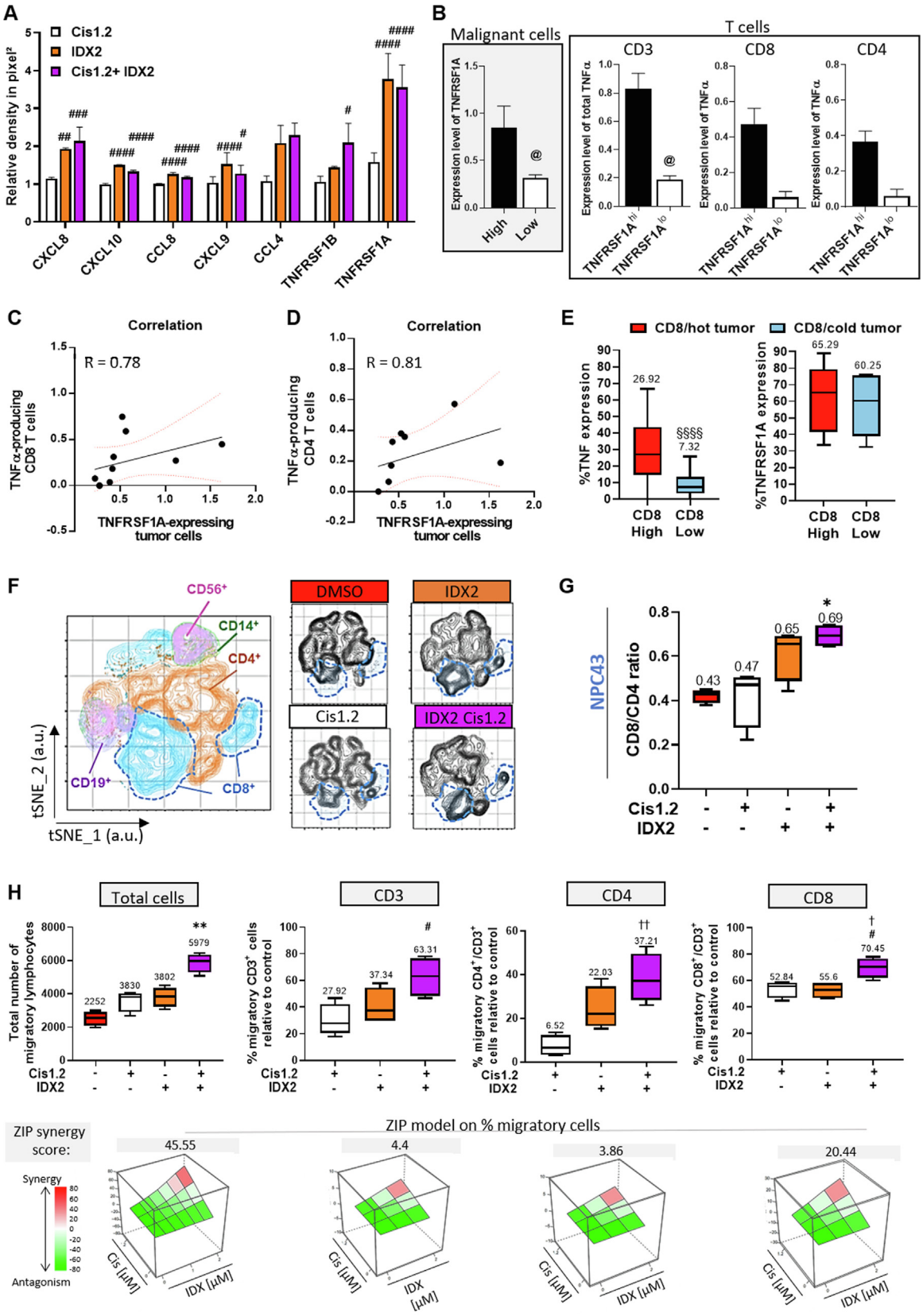
A
Cis1.2
IDX2
Cis1.2+ IDX2
Relative density in pixel²
CXCL8
CXCL10
CCL8
CXCL9
CCL4
TNFRSF1B
TNFRSF1A
B
Malignant cells
Expression level of TNFRSF1A
High
Low
T cells
CD3
CD8
CD4
Expression level of total TNFα
Expression level of TNFα
TNFRSF1A hi
TNFRSF1A lo
C
Correlation
R = 0.78
TNFα-producing CD8 T cells
TNFRSF1A-expressing tumor cells
D
Correlation
R = 0.81
TNFα-producing CD4 T cells
TNFRSF1A-expressing tumor cells
E
CD8/hot tumor
CD8/cold tumor
%TNF expression
26.92
7.32
%TNFRSF1A expression
65.29
60.25
CD8 High
CD8 Low
F
CD56⁺
CD14⁺
CD4⁺
CD19⁺
CD8⁺
tSNE_2 (a.u.)
tSNE_1 (a.u.)
DMSO
IDX2
Cis1.2
IDX2 Cis1.2
G
NPC43
CD8/CD4 ratio
0.43
0.47
0.65
0.69
Cis1.2
IDX2
H
Total cells
CD3
CD4
CD8
Total number of migratory lymphocytes
% migratory CD3⁺ cells relative to control
% migratory CD4⁺/CD3⁺ cells relative to control
% migratory CD8⁺/CD3⁺ cells relative to control
2252
3830
3802
5979
27.92
37.34
63.31
6.52
22.03
37.21
52.84
55.6
70.45
ZIP synergy score:
Synergy
Antagonism
ZIP model on % migratory cells
45.55
4.4
3.86
20.44
Cis [μM]
IDX [μM]

treatment through three-way comparisons (phenotype, cytokine production and transcriptional regulation). Circulating memory *T*-cell populations in humans are often distinguished based on expression of CD45RA and CD62L, wherein CD45RA^{lo}CD62L^{hi} cells are considered Tcm and CD45RA^{lo}CD62L^{lo} are Tem [6,28]. Utilizing this paradigm to differentiate subsets of human memory CD8$^+$ T cells, we noted a considerable increase in the proportion of Tem population in response to the combination treatment. In contrast, a trend towards a reduced frequency of Tcm was found (Fig. 3A-C). The preferential differentiation of CD8$^+$ Tem cells observed in NPC43 co-cultures compared to C17 tumor cells was presumably due to their higher ENOX2 expression levels, and was consistent with our previous observations.

In addition to the increased frequency, the CD8$^+$ Tem cells also expressed relatively higher levels of TNFα, but not IFNγ or IL-2, in the combined treatment group as compared to control (Fig. 3D-E). Therefore, the combination treatment not only increased the expression of TNFRSF1A by NPC cells as described previously, but also increased TNFα production by CD8$^+$ Tem cells in the co-culture, further suggesting that the combination treatment could potentially promote TNFα-TNFRSF1A interaction in the TME. This activated functional state associated with Tem was further confirmed by distinct transcriptional differences, including expression of elevated levels of Tem-signature molecules such as *CCL5* and reduced levels of Tcm-signature molecules *CXCR3* in the co-cultures of the combination treatment group (Fig. 3F). Sphingosine-1 phosphate receptors (S1PR) were previously reported to be highly regulated during human *T*-cell differentiation. In fact, we found an increased expression of *S1PR5*, a Tem cell-associated receptor, in the co-treatment group (Fig. 3G), confirming that the action of IDX in combination with Cis favors Tem-like phenotype differentiation.

The transcriptome profiles of Tem and Tcm were compared between 10 NPC tumor-blood pairs from single-cell data publicly available (GSE162025) and our NPC tissues dataset (GSE150825). Focusing on the CD8$^+$ subpopulations, we observed characteristic features of Tem, with a gene signature including *CX3C1*, *KLRG1*, *S1PR5*, *FGFBP2* and *KLF2*. The relationship analyses of memory *T*-cell populations revealed the dramatic rarity of both Tcm and Tem subsets within tumor tissues, with most memory T cells present in the periphery instead. This limited memory *T*-cell profile within tumor tissues was also confirmed by our scRNA-Seq data. (Fig. 3H). These findings suggested that the observed low infiltration of memory T cells might largely affect *T*-cell immunity against NPC.

The combination treatment promotes Tem–mediated cytotoxicity with preferential sustainable HIF expression and accelerated granzyme B production against ENOX2-high tumor cells

Given the fact that the CD8$^+$ *T*-cell transition into memory subsets was more skewed to Tem than Tcm upon combination treatment, we further investigated the functional characterization of these memory *T*-cell subpopulations. We found that the gene (Supplementary Fig. 6B) and protein expression of granzyme B, a key effector molecule for the killing of tumor cells, by CD8$^+$ T cells were greatly increased after the combination treatment (NPC43 co-cultures, Fig. 4A; C17 co-cultures Supplementary Fig. 6A). The same observation was made for CD8$^+$ Tem (Fig. 4B). To demonstrate that we were measuring *de novo* produced granzyme B, rather than residual unreleased granzyme B, within responding cells, we co-stained the cells during stimulation with anti-CD107a to assess degranulation. Up-regulation of CD107a expression in CD8$^+$ T cells from the co-treatment group was observed, compared to the DMSO control group (Supplementary Fig. 6C). Since granzyme B could play either a tumoricidal or tumorigenic role depending on the niche, we further explored whether the induced granzyme B could exert cytotoxic effects toward tumor cells. ΔΨm is an indicator of cell health, and the dissipation of ΔΨm suggests a loss of mitochondrial membrane integrity, reflecting the initiation of a pro-apoptotic signal. JC-1 staining was performed to measure ΔΨm, using the ratio between red fluorescent aggregates and green fluorescence monomers. There was a significant increase in monomer/aggregate fluorescence intensity ratio in the co-treatment group, compared with the control group (Fig. 4C). Additionally, the ATP detection-based CellTiter Glo assay indicated decreased ATP content in tumor cells treated with IDX in combination with Cis (Supplementary Fig. 6D). Besides, C17 tumors responded less strongly to the combination therapy. Whilst the same trend was observed, statistical significance was not reached. Upon combination treatment, these immune activities differ, where stronger responses were observed in tumor cells with higher ENOX2 expression compared to those displaying lower ENOX2 expression levels, suggesting that combined treatment effectiveness is strongly correlated with the availability of the ENOX2 target on the surface of cancer cells.

In line with our previous observation, we confirmed that co-treatment induced granzyme B production in co-cultured tumor cells by Western blotting, suggesting that the cytolytic molecule could enter the target cells (third lane; Fig. 4D). Additionally, the

Fig. 2. A synergistic *T*-cell migration induced by combined treatment of IDX and Cisplatin. (**A**) Antibody array analysis of inflammatory cytokines in conditioned media from NPC43 following treatment with IDX, Cis or combinations of both. Quantitation of relative fold induction of cytokines compared with DMSO control cells were measured. (**B**) Single-cell transcriptomics (GSE150430) reveals TNFRSF1A as high and low expression of malignant cells in NPC tissues (median cut-off value). TNFα-expressing T cells, CD8 and CD4 T cells within tumor tissues were quantified from the high (TNFRSF1A^{hi}) and low (TNFRSF1A^{lo}) subgroup. (**C**) Correlation between TNFRSF1A-expressing tumor cells and TNFα-expressing CD8 T cells. (**D**) Correlation between TNFRSF1A-expressing tumor cells and TNFα-expressing CD4 T cells. (**E**) The degree of CD8$^+$ T cell infiltration in tumors defines CD8 high/ "hot" tumor or CD8 low/cold tumor. The percentage expression levels of TNFα and TNFRSF1A were quantified in high and low groups. (**F**) *t*-SNE analysis of concatenated mononuclear cells (3,000 cells/sample) from PBMCs collected from NPC43 and C17 co-cultures. *T*-SNE represent phenotypic markers defining specific cells and are assigned specific colors (CD19 B cells in purple; CD56 natural killer cells in pink; CD14 monocyte in green; CD4 T helper cells in orange; CD8 cytotoxic T cells in blue). Distinct differential expression CD8 T cells are highlighted in blue broken line. (**G**) CD8/CD4 ratio was calculated according to the cellular percentage changes with (+) or without (-) indicated drug treatment from flow cytometric analysis. (**H**) Effect of IDX and Cis on *T*-cell migration. Leukocytes migration towards NPC43 cell lines following IDX and Cis treatments alone or combined were measured by flow cytometry. Migration of total leukocytes were measured by CD45. Specific migratory effects of the % CD3 T cells/CD45 cells, % CD4 helper T cells/CD3 cells and % CD8 cytotoxic T cells/CD3 cells were compared to control (DMSO). The interaction landscape between two drugs was calculated using ZIP model. Data information: Data points are shown ± SEM. In the boxplots in (E, G, H), the centerline indicates the median, while the upper and lower lines represent the 75th and 25th percentiles, respectively. The whiskers represent the smallest and largest values in the 1.5 × interquartile range. Values on top indicate median. In (A, G, H), P values were calculated using unpaired Kruskal–Wallis test without multiple comparison correction. In (B, E), P values were analyzed with unpaired Mann–Whitney test. In (C, D), statistical evaluations were performed using Spearman's rank correlation test. @p < 0.05 compared to TNFRSF1A; §§§§p < 0.0001 compared to CD8/hot tumor; *p < 0.05, **p < 0.01 compared to medium alone; #p < 0.05, ####p < 0.0001 compared to Cis1.2; † p < 0.05, ††p < 0.01 compared to IDX2.

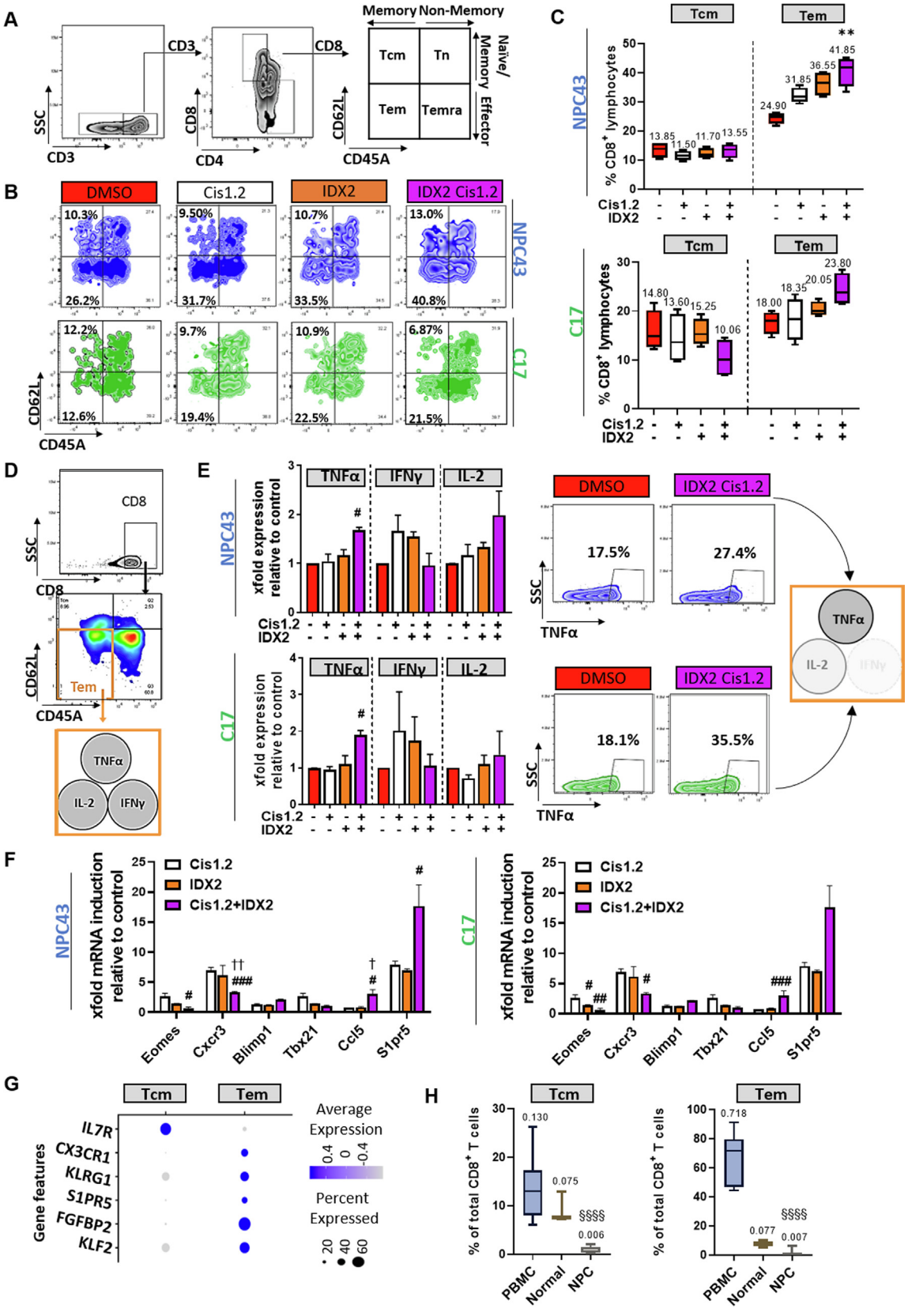
A
CD3
CD8
CD4
CD45A
Memory Non-Memory
Tcm
Tn
Tem
Temra
Naïve/ Memory Effector
B
DMSO
Cis1.2
IDX2
IDX2 Cis1.2
NPC43
C17
10.3%
26.2%
9.50%
31.7%
10.7%
33.5%
13.0%
40.8%
12.2%
12.6%
9.7%
19.4%
10.9%
22.5%
6.87%
21.5%
C
Tcm
Tem
% CD8+ lymphocytes
13.85
11.50
11.70
13.55
24.90
31.85
36.55
41.85
14.80
13.60
15.25
10.06
18.00
18.35
20.05
23.80
D
CD8
Tem
TNFα
IL-2
IFNγ
E
xfold expression relative to control
TNFα
IFNγ
IL-2
17.5%
27.4%
18.1%
35.5%
F
xfold mRNA induction relative to control
Cis1.2
IDX2
Cis1.2+IDX2
Eomes
Cxcr3
Blimp1
Tbx21
Ccl5
S1pr5
G
Gene features
IL7R
CX3CR1
KLRG1
S1PR5
FGFBP2
KLF2
Average Expression
Percent Expressed
H
% of total CD8+ T cells
0.130
0.075
0.006
0.718
0.077
0.007
PBMC
Normal
NPC

granzyme B-induced killing effect was found to be dependent on caspase signaling and that intact type I IFN signaling in cancer cells, was maintained after Cis treatment and further activated upon combination with IDX. Hypoxia induced factor (HIF) is widely considered to not only sustain glycolysis in $CD8^+$ T cells but also allow for the generation of inflammatory mediators such as granzymes. Supporting this notion, the co-treatment enhanced the production of HIF1α in tumor cells (second lane; Fig. 4D). Notably, addition of an antioxidant, NAC, suppressed granzyme B production in $CD8^+$ T cells, supporting that HIF1α is essential to confer cytotoxicity to T cells (Fig. 4E). In light of these observations, we postulated that combination of IDX/Cis promoted cytotoxicity and anti-tumor properties *via* induction of granzyme B-producing T cells, mediated, at least in part, through a hypoxia stress-associated pathway. A subsequent cell-mediated cytotoxicity assay at the highest effector:target (E:T) ratio of 20:1 demonstrated an approximate 3-fold elevated synergistic cytotoxicity in the combination treatment with IDX and Cis, when compared to the DMSO control group (Fig. 4F). This increased cell-mediated cytotoxicity was commensurate with an observed differentiation of the $CD8^+$ T cells towards an effector phenotype upon co-treatment. Taken together, the co-treatment predisposes a specific niche within the TME which is likely to augment the *T*-cell mediated cytotoxic activity against cancer cells (Fig. 4G).

Combination therapy synergistically increases *T*-cell infiltration and mediates apoptosis in NPC-derived spheroids

NPC43, which expressed high levels of ENOX2, was able to elicit a superior response to the combination therapy, showing increased $CD8^+$ Tem mobilization, differentiation and a higher amount of lysed tumor cells in *in vitro* 2D cultures experiments. We thus selected this tumor cell line to mimic *in vivo* conditions to study the cytotoxic effects of the combination treatment using 3D tumor spheroids. Having established the optimal conditions for spheroid assembly (Supplementary Fig 7A), we assessed increasing concentrations of IDX and Cis on apoptosis using fluorescent probes (non-toxic CellEvent Caspase-3/7 Green) in combination with bright-field microscopy, to perform real-time spheroid imaging (Supplementary Fig 7B). The drug effect in the 3D "CellEvent," was used to build a dose–response curve and determine the IC_{50} values for Cis at 1.4 μM and IDX at 2.1 μM (Fig. 5A). Overall, the IC_{50} values were comparable between the spheroid-derived cells in 3D and 2D conditions.

Spheroids generated from an NPC cell line were co-cultured with PBMCs obtained from healthy donors that were HLA-matched whenever possible, to evaluate the interactions between tumor spheroids and PBMCs through heterotypic co-cultures. After co-culture, the cellular composition within infiltrated tumor spheroids was determined by mechanically separating infiltrating cells (IN) from those cells remaining in the medium (OUT) (Fig. 5B). As expected, it was found that PBMCs preferentially localized close to the tumor spheroid in the IDX/Cis drug combination (Fig. 6B). This increase in PBMC infiltration into the tumor spheroids following treatment was rapid and detected as early as 2 h following the initiation of co-culture, while the number of infiltrating cells remained constant in the controls (DMSO) over 72 h of co-culture. The combination treatment resulted in elevated infiltrating PBMCs (total immune cells per spheroid, mean 164.5 ± 4.5) when compared to Cis alone (mean 53.0 ± 6.0), representing a significant ($p = 0.0149$) 3.1-fold increase (Fig. 5C and Supplementary Fig. 5C). Strikingly, PBMC infiltration in cis-treated tumor spheroids started to decline after 24 h of incubation. The functional consequences of this immune cell infiltration and activation in spheroids were explored by live-imaging and flow cytometry. The spheroid destruction was correlated to an active apoptosis process in tumor cells, involving global activation of caspase-3 and −7 (CellEvent staining; Fig. 5D). The immunomodulatory effects of IDX in conjunction with Cis on cell infiltration and tumor destruction was analyzed by the ZIP model and a synergistic effect was observed with co-treatment (Fig. 5E), confirming the immunomodulatory property of IDX as one of the drugs combination-induced anticancer activities. Focused analysis on the drug combination group and the DMSO control demonstrated a trend toward higher proportions of TIL-CD3 in the spheroid upon co-treatment (Fig. 5F). In this context, phenotypes of TIL-CD8 appeared to be impacted by the combination treatment with a loss of CD45RA and CD62L, resulting in increased $CD8^+$ Tem observed inside the spheroids (Fig. 5F). This demonstrated the capacity of T cells to react toward the tumor cells upon combined treatment with IDX and Cis and confirmed our previous observations of an increased functionality of Tem cells as compared to other *T*-cell subsets.

Combination therapy induces a TME with stronger *T*-cell immune phenotype promoting superior anti-tumor response

The addition of IDX demonstrates an enhanced direct cytotoxicity of Cis against NPC cell lines *in vitro*. To verify such activity *in vivo*, nude mice bearing NPC43 cell line-derived xenografts were treated every-other-day with IDX (10 and 20 mg/kg) and/or Cis (5 mg/kg). Using this model, the high combination-treatment (IDX20 + Cis5) resulted in a significant reduction in tumor growth, compared to the control group (Supplementary Fig 8A-B).

Given that the observed *in vitro* synergistic anti-tumor effects of IDX/Cis drug combination are likely mediated by the presence of Tem cells, we further assessed this protective efficacy using a three-step humanized mouse model. Immunodeficient mice were first humanized by transplanting human $CD34^+$ hematopoietic

Fig. 3. Combined treatment with IDX and Cisplatin drives CD8 *T*-cell differentiation into Tem phenotype. (A) Gating strategy to identify the principal $CD8^+$ *T*-cell subsets. CD8 gated cells were then separated into 4 subsets (Tn, Tcm, Tem, Temra) based on CD45RA and CD62L labeling. **(B)** Representative flow cytometry plots demonstrating the frequency of $CD8^+$ Tcm ($CD62L^{hi}$) and Tem ($CD62L^{lo}$) within PBMCs on day 5 of co-cultures (NPC43, blue; C17, green). **(C)** Frequency of $CD8^+$ Tcm and Tem by indicated drugs [with (+) or (without)], alone or in combination was analyzed by flow cytometry and quantified. **(D)** $CD8^+$ Tem gated cells were analyzed for the assessment of TNFα, IFNγ, IL-2 production in the co-cultures. **(E)** Representative flow cytometry plots (right) and quantification of the frequency of cytokine production by Tem. Summary of cytokine production: grey gradient indicates the strength of data support (darker grey representing stronger evidence, dotted line showing lower level of evidence in relation to the control upon combination treatment). **(F)** qRT-PCR of mRNA expression of indicated genes from PBMC co-cultures upon IDX, cisplatin (cis), alone or in combination. Graphs representing relative gene expression data (ddCt) determined by q-RT-PCR on indicated genes relative to beta-actin. **(G)** A single-cell transcriptome analysis (GSE162025 and GSE150825) on differential expression of transcription factors predicted to regulate central (Tcm) and effector memory *T*-cell (Tem) states. **(H)** Proportion of Tem and Tcm frequency in paired NPC tumor-blood samples (GSE162025) and NPC tissues (GSE150825). Data information: Data points are shown ± SEM. In the boxplots in (C, H), the centerline indicates the median, while the upper and lower lines represent the 75th and 25th percentiles, respectively. The whiskers represent the smallest and largest values in the 1.5 × interquartile range. Values on top indicate median. In (C, E, F. H), P values were calculated using unpaired Kruskal–Wallis test without multiple comparison correction. $^{**}p < 0.01$ compared to medium alone; #$p < 0.05$, ###$p < 0.001$ compared to Cis1.2; †$p < 0.05$, ††$p < 0.01$ compared to IDX2; §§§§ $p < 0.0001$ compared to peripheral blood mononuclear cells (PBMC) from NPC patients.

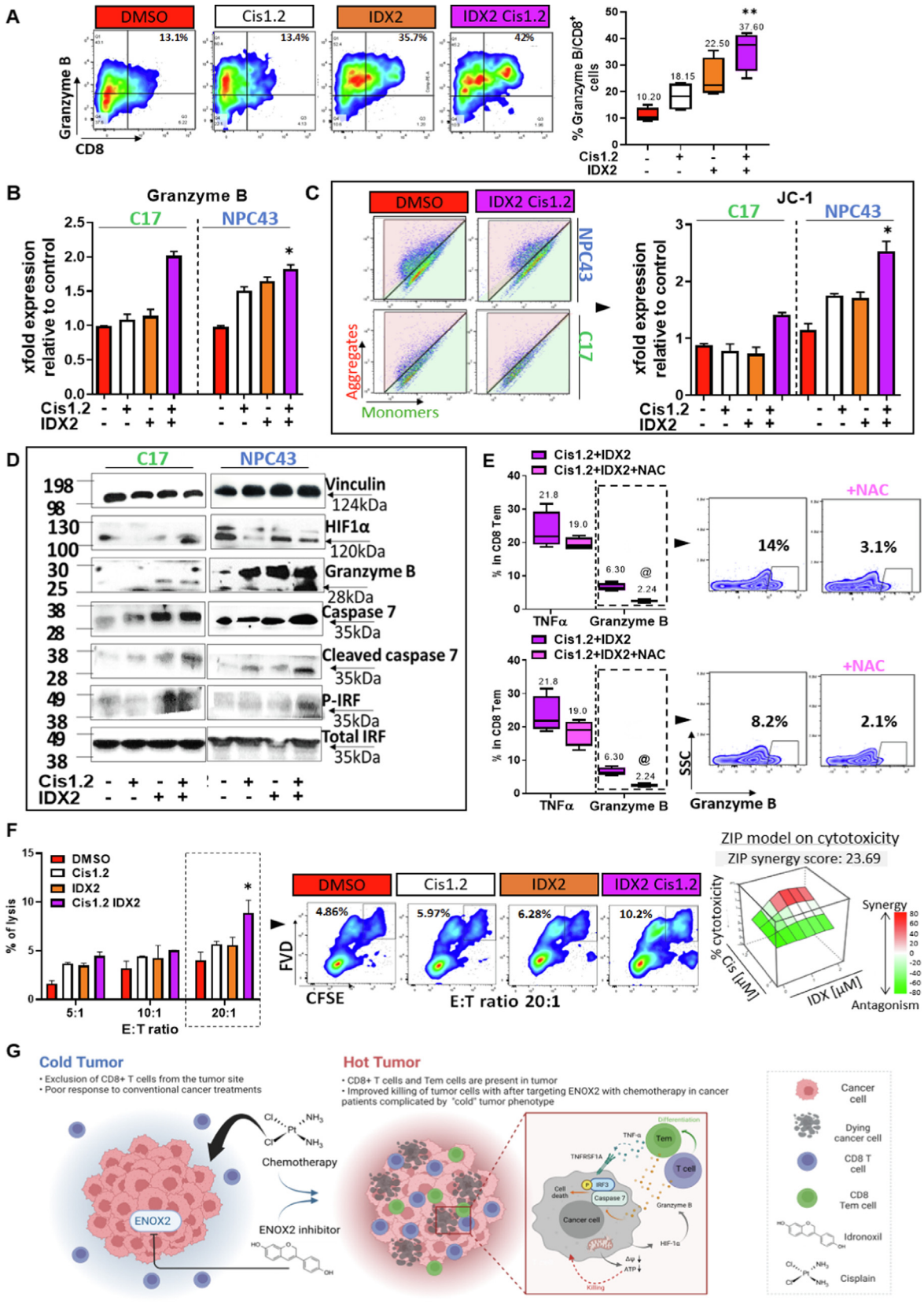
A
DMSO
Cis1.2
IDX2
IDX2 Cis1.2
13.1%
13.4%
35.7%
42%
Granzyme B
CD8
% Granzyme B/CD8+ cells
10.20
18.15
22.50
37.60
Cis1.2
IDX2
B
Granzyme B
C17
NPC43
xfold expression relative to control
C
DMSO
IDX2 Cis1.2
Aggregates
Monomers
JC-1
D
Vinculin 124kDa
HIF1α 120kDa
Granzyme B 28kDa
Caspase 7 35kDa
Cleaved caspase 7 35kDa
P-IRF 35kDa
Total IRF 35kDa
E
Cis1.2+IDX2
Cis1.2+IDX2+NAC
% in CD8 Tem
TNFα
Granzyme B
+NAC
14%
3.1%
8.2%
2.1%
SSC
F
DMSO
Cis1.2
IDX2
Cis1.2 IDX2
% of lysis
E:T ratio
5:1
10:1
20:1
FVD
CFSE
4.86%
5.97%
6.28%
10.2%
E:T ratio 20:1
ZIP model on cytotoxicity
ZIP synergy score: 23.69
% cytotoxicity
% Cis [μM]
IDX [μM]
Synergy
Antagonism
G
Cold Tumor
• Exclusion of CD8+ T cells from the tumor site
• Poor response to conventional cancer treatments
Hot Tumor
• CD8+ T cells and Tem cells are present in tumor
• Improved killing of tumor cells with after targeting ENOX2 with chemotherapy in cancer patients complicated by "cold" tumor phenotype
ENOX2
Chemotherapy
ENOX2 inhibitor
Cancer cell
Dying cancer cell
CD8 T cell
CD8 Tem cell
Idronoxil
Cisplain

stem cells, that differentiate into functional human lymphocytes, then implanted them with a NPC43 cell xenograft, before treating them with IDX (15 mg/kg) and/or Cis (2.5 mg/kg) four times per week (Fig. 6A). Combined treatment displayed the strongest tumor volume inhibition, with inhibitory rates of 56 %, 82 % and 106 % for the IDX, Cis and combined treatment groups, respectively (Fig. 6B); data that is consistent with our findings in the nude mouse model. Additionally, the tumor weight at the end of study was significantly reduced by the combined treatment compared to the DMSO control group (Fig. 6C).

Using this humanized *in vivo* platform, we set out to characterize the NPC TME with emphasis placed upon T cell characterization. Despite a broad range of humanization rates (determined by human lymphocytes; Supplementary Fig 8C) that resulted in a high variability in the percentages of both tumor infiltrating lymphocytes (TILs) and systemic lymphocytes (SLs), the ratio between TILs and SLs remained consistent (Supplementary Fig 8D). To mitigate this variability, all subsequent analysis was therefore carried out using the TIL to SL ratio (TIL/SL). As expected, tumor tissues were enriched with $CD3^+$ T cells in the combination treatment group compared to the DMSO group, as determined by the increased $CD3^+$ TIL/SL (Fig. 6D).

We identified that all *T*-cell differentiated subsets (Tn, Tcm, Tem and Temra) were present in the SLs, whereas only Tcm and Tem were present within the TIL population (Supplementary Fig 8E). Furthermore, combination treatment increased the TIL/SL ratio for Tem (CD4 and CD8), but an opposite effect was observed for Tcm (CD4 and CD8; Fig. 6E). These results further strengthened our *in vitro* finding that in addition to phenotypic alterations to Tem, Tem tend to infiltrate more than Tcm within the TME after co-treatment with IDX and Cis. We extended this interpretation by comparing the systemic response to the treatment (post-treatment to pre-treatment ratio). We found a reduction in Tem frequencies (CD4 and CD8), whereas Tn showed an increased level upon combination treatment (Fig. 6F for CD8, Supplementary Fig 8F for CD4). This systemic change led us to hypothesize that the combination treatment would induce an infiltration of Tem cells from the peripheral compartments into the tumor nest, resulting in reduced systemic Tem. In this context, Tn cells are likely to be elevated as a replacement for homeostatic systemic supply.

A correlation between tumor weight and TIL/SL ratio was observed (Fig. 6G). Increased tumor weight was correlated with a substantial decrease in $CD3^+$ TIL/SL ratio ($p < 0.0397$), with an increase in the $CD8^+$ Tcm ($p < 0.0168$) and a decrease in the Tem ($p = 0.0535$) subset. A positive correlation with tumor weight was also found in the $CD4^+$ Tcm, but not $CD4^+$ Tem (Supplementary Fig 8G). Collectively, the combination treatment demonstrated a therapeutic effect along with enhanced trafficking of lymphocytes from the peripheral compartments into the tumor, that was associated with the $CD8^+$ Tem subset and decelerated tumor growth.

Discussion

Current treatments of NPC usually involve cytotoxic chemotherapies, however, their efficacy is often restricted by various immune parameters pre-established in the TME [29]. In addition to the suppressive immune microenvironment, tumor-associated ENOX2 presence and relative expression level is largely proportional to tumor burden, providing a potential biomarker for response to therapy and disease progression [30]. While several early-phase trials of the ENOX2 inhibitor, IDX, in combination with chemotherapy have reported its safety, tolerability and potential efficacy in solid cancers, the associated immunological mechanisms remain largely unknown. In contrast to previous published studies that focus on cancer cell-associated apoptosis or immune cell-induced inflammation by targeting ENOX2, this study addresses the impact of a combination strategy targeted to ENOX2 with chemotherapy for inducing TME inflammation via immune-cell/target-cell interaction. Our data reveal a significant function which, to our knowledge, has never been previously explored.

Here, we demonstrate that NPC cancers mainly exert a *T*-cell-excluded tumor phenotype, with active *T*-cell exclusion from the tumor parenchyma and retention of these cells within the tumor stroma, which characterizes an immunologically "cold-tumor" [9,25]. This "cold-phenotype" is closely associated with those cohorts expressing higher levels of intra-tumoral ENOX2. In our model, cisplatin combined with IDX drove "cold-NPC" tumors into an immunologically "hot-tumor" state. In fact, strong immunostimulatory response was preferentially elicited by tumor cells with high- over low-ENOX2 expression following combination treatment. The impact of this therapeutic combination was shown to be directly related to an underlying immunogenic vulnerability, such that combined treatment increased migration of $CD8^+$ T cells into the tumor, enhanced the naive-to-effector memory $CD8^+$ *T*-cell transition, leading to cytolytic Tem-mediated immune response that was able to infiltrate into the TME and curb tumor growth in NPC animal models. We postulate that $CD8^+$ Tem–mediated enhancement of tumor death upon combination therapy might be directly correlated to higher levels of ENOX2 expression that "help" elicit heightened inflammation. The data suggest that

Fig. 4. HIF1α-mediated granzyme B production from T cells contributes to the synergy of cytotoxicity in combined treatment with IDX and Cis. (A) Representative flow cytometry plots (left) and quantification of the frequency of granzyme B production by $CD8^+$ T cells from NPC43 co-cultures with (+) or without (-) indicated drugs. (**B**) Quantification of the frequency of granzyme B production by $CD8^+$ Tem cells from NPC43 and C17 co-cultures. (**C**) JC-1 staining of target tumor cells shows reduction in mitochondrial membrane potential (Ψm) after combination treatment. Flow cytometry dot plot showing the gating of JC1 (red)-aggregates and JC1 (green)-monomer populations, while bar graphs show the ratio of JC-1 monomers to aggregates eomesfor experimental groups. (**D**) Immunoblots of co-cultured NPC43 and C17 tumor cells with PBMCs for 3 days with control (DMSO) or IDX and Cis, alone or in combination for 3 days. (**E**). Representative flow cytometry plots (left) and quantification of the frequency of granzyme B production by $CD8^+$ T cells from NPC43 co-cultures upon combination therapy. (**F**) Quantitative data of % lysis (in terms of $CFSE^+FVD^+$ cells) was obtained (left). Representative flow cytometry plots (middle) of NPC43 cell (target cell; T) stained with CFSE before getting in contact with PBMCs (effector cell; E) collected from co-cultures at indicated effector:target ratio (E:T) for 3 days. Cells were then collected and stained with fixable viability dye (FVD) and the dead cells (%) were measured by flow cytometry. $CFSE^+$ cells are target cells and FVD + cells are dead cells, such that dead target cells are represented by the $CFSE^+FVD^+$. The interaction landscape between two drugs was calculated using ZIP model (right). (**G**) Working model depicting the interaction of IDX/Cis and memory *T*-cell-mediated cytotoxicity as an anti-tumor mechanism in NPC cancer cells. Combination treatment potentiate migration of $CD8^+$ T cells and skew towards Tem differentiation with enhanced release of granzyme B. Co-treatment induce hypoxic environment *via* production of HIF1α, which in turn potentiate the granzyme B production and evoke cell-mediate cytotoxicity including mitochondria dysfunction. A possible amplification mechanism could be due to the elevated TNFRSF1A expression in target cells and TNFα production from effector Tem cells upon co-treatment. Solid arrow depicts identified roles from current study and dashed arrows represent possible mechanisms or connections (created with BioRender.com). Data information: Data points are shown ± SEM. In the boxplots in (A, E), the centerline indicates the median, while the upper and lower lines represent the 75th and 25th percentiles, respectively. The whiskers represent the smallest and largest values in the 1.5 × interquartile range. Values on top indicate median. In (A, B, C, F), P values were calculated using unpaired Kruskal–Wallis test without multiple comparison correction. In (E) data were analyzed with unpaired Mann–Whitney test. *$p < 0.05$, **$p < 0.01$ compared to medium alone; @$p < 0.05$ compared to Cis1.2 + IDX2.

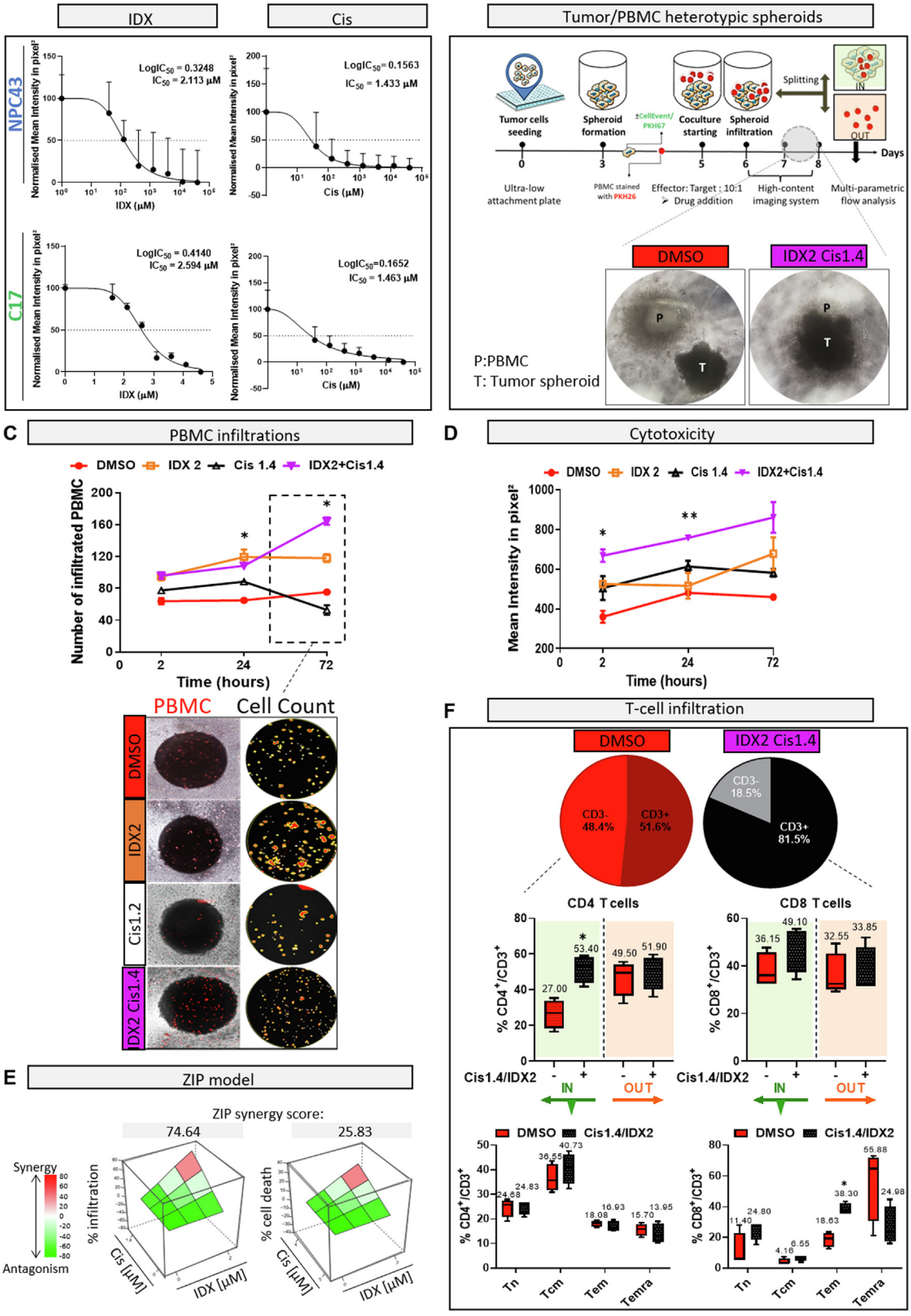
IDX
Cis
NPC43
C17
Normalised Mean Intensity in pixel²
LogIC50 = 0.3248
IC50 = 2.113 µM
LogIC50= 0.1563
IC50 = 1.433 µM
LogIC50 = 0.4140
IC50 = 2.594 µM
LogIC50=0.1652
IC50 = 1.463 µM
IDX (µM)
Cis (µM)
Tumor/PBMC heterotypic spheroids
Tumor cells seeding
Spheroid formation
±CellEvent/ PKH67
Coculture starting
Spheroid infiltration
Splitting
IN
OUT
Days
Ultra-low attachment plate
PBMC stained with PKH26
Effector: Target : 10:1
Drug addition
High-content imaging system
Multi-parametric flow analysis
DMSO
IDX2 Cis1.4
P:PBMC
T: Tumor spheroid
C
PBMC infiltrations
DMSO
IDX 2
Cis 1.4
IDX2+Cis1.4
Number of infiltrated PBMC
Time (hours)
PBMC Cell Count
D
Cytotoxicity
Mean Intensity in pixel²
E
ZIP model
ZIP synergy score:
74.64
25.83
Synergy
Antagonism
% infiltration
% cell death
Cis [µM]
IDX [µM]
F
T-cell infiltration
CD3- 48.4%
CD3+ 51.6%
CD3- 18.5%
CD3+ 81.5%
CD4 T cells
CD8 T cells
% CD4+/CD3+
% CD8+/CD3+
Cis1.4/IDX2
IN
OUT
% CD4+/CD3+
% CD8+/CD3+
Tn
Tcm
Tem
Temra

chemotherapy with an ENOX2-targeted drug act synergistically, resulting in immunogenic cell death which is essential to overcome high ENOX2-associated non-*T*-cell-inflamed "cold" cancers, such as NPC.

Our research group [23] previously demonstrated the importance of spatial context and the nature of cellular heterogeneity of the TME, beyond overall densities, that may provide additional contextual information relevant to cancer immunity. Furthermore, it has been suggested that immune topographies (infiltration pattern) can be used as independent biomarkers for patient selection for immunotherapy responses in certain types of cancers [29,31]. Thus, an improved understanding of the immune signature of tumors is essential to guide the design of scientific and clinical combination studies, that may succeed in transforming non-responsive cancers into responsive phenotypes. We suggest that ENOX2 is ideally suited as a target for early diagnosis of cancer as this protein not only strongly expressed on the cell surface of malignancy, its expression is potentially associated with tumor phenotypes. To our knowledge, this study is the first to demonstrate that surface-expressed ENOX2 levels in the tumor-region, rather than total frequency in tumor islet, can be associated with TIL-CD8 densities. This spatial feature between ENOX2 and CD8 T cells allows better understanding on how the TME architecture influences outcomes in NPC. Moreover, we believe that the spatial information is could be key to improve patient stratification, as such, patients with high level of cancer-specific ENOX2 may require specific strategies, such as combination of IDX to chemotherapy, to increase T cell infiltration into the tumor. In this study, our approach, using ENOX2 as a target for NPC intervention exerts synergistic effect in combining with chemotherapy, as determined by both the quantity and quality of responses. These responses are likely dependent on the phenotypic, functional and localization properties of the memory *T*-cell compartments.

Human memory T cells with discrete lymphoid homing properties were first described by Sallusto et al. [6], yielding the definition of canonical memory *T*-cell subsets, Tcm and Tem. General features of Tcm include greater proliferative capacity and heightened presence in secondary lymphoid organs. A high frequency of T cells found in nonreactive lymph nodes have the Tem phenotype, which is considered to be more cytolytic and has a greater capacity of trafficking toward infected sites [28,32]. Therefore, categorization of memory T cells into distinct lineages provides a division of labor as well as flexibility in the mounting of robust defenses against diverse pathogens and cancers. This study demonstrates that Cis alone is able to increase *T*-cell migration, but this treatment alone is not sufficient to overcome the barrier of "cold" tumors and provide robust patient responses. The addition of IDX can improve local infiltration and activity of T cells, promote differentiation of $CD8^+$ Tem cells, skew the memory pool and impact functional cytotoxic immunity.

Since the functions of locally secreted soluble factors, such as cytokines and chemokines, are increasingly recognized in cancers, we hypothesize that IDX in combination with Cis may lead to the induction of bioactive mediators in the TME that are pivotal for influencing *T*-cell immunity in NPC. We observed increased levels of inflammatory-related cytokines in the CM of tumor cultures, in particular upon combination treatment. Therefore, in our point of view, these increased tumor-derived mediators encountered within the TME may represent a pro-inflammatory milieu, potentially interacting closely with anti-tumor *T*-cell populations. The cell–cell interaction analysis suggests that several outgoing signals from tumor cells to *T*-cell receivers are enriched in the TME of NPC. Notably, most of the enriched outgoing signals are not *via* those mediators observed in the CM collected from combined-treated NPC cells. This finding suggests that the combination therapy can drive a distinct pro-inflammatory TME (senders) and further boost the recruitment of *T*-cell populations (receivers) with antitumor immunity. The ligand–receptor pairs between tumor cells and TME-infiltrated T cells, influenced by the combination treatment, are worthy of further research as a potentially modifiable contributor to tumor immunophenotype.

A killing mechanism used by cytotoxic lymphocytes involves proteases (granzymes) translocating into the cytoplasm of the target cell, resulting in its death. Granzyme B is the best characterized serine protease, is widely used as an activation marker of cytotoxic T cells and is a potent cytotoxin mediating target cell apoptotic death [33]. Mitochondria appear to be dysregulated in granzyme B-mediated apoptosis [34]. In fact, here we identify a potential association between granzyme B and mitochondria dysfunction upon combination treatment, with this dysregulation likely due to the reduced $\Delta\Psi m$ and ATP production, leading to cellular demise through a caspase-dependent mechanism. This is in line with the findings of previous studies, suggesting that Tem exhibit an effector phenotype marked by granzyme production [35].

Hypoxic conditions are typically present in solid tumors. It is intriguing, and perhaps counterintuitive, that the release of HIF1α, an oxygen-sensitive transcriptional activator, would drive therapeutic benefit in NPC. Nonetheless, it has been well documented that cytolytic functions of T lymphocytes respond to the immune microenvironment and tissue oxygenation levels. That response in turn is regulated, to a significant degree, by HIF1α [36,37]. As such, our proposal is a mechanism by which the increased granzyme B-producing $CD8^+$ Tem cells, likely driven by the secretion of HIF1α from tumor cells upon combined drug treatment, favors the accumulation of granzyme B in the TME and potentiates the response of memory cytolytic subsets that are necessary to increase tumor death. In support of these findings, other studies have also demonstrated that the presence of HIF1α not only increases the generation of cytolytic molecule granzyme B [36], but also supports *T*-cell acquisition into an effector phenotype

Fig. 5. High-content monitoring of drug effects in a 3D spheroid model upon combination treatment. (A) CellEvent was used to determine the IC_{50} values for IDX and Cis in NPC43 spheroids. **(B)** Scheme of the co-culture protocol between NPC spheroids and PBMCs from healthy donors. Spheroids were pre-formed for 5 days with 20,000 cells/well and then co-cultured with PBMCs for 3 days with indicated drugs. Representative images were acquired using the InCell 6000. Lymphocytes IN (green) and OUT (orange) spheroid compartments were quantified by flow cytometry. **(C)** PKH26-stained and CellEvent-stained spheroids were co-cultured. Numbers of infiltrated cells at indicated times were calculated by Fuji ImageJ software. **(D)** Apoptotic tumor cells were measured according to CellEvent intensity. **(E)** The interaction landscape between two drugs on the degree of infiltration (left) and cell death (right) was calculated using ZIP model. **(F)** Flow cytometry analyses of T cells (respectively gated $CD3^+$; pie plot) as well as $CD4^+$ and $CD8^+$ T cells subsets (respectively gated $CD4^+CD8^-$ among $CD4^-CD8^+$ among $CD3^+$; bar plots inside rectangle box) in the IN (green) and OUT (orange) compartments, in the presence or without co-treatment at 72 h. Flow cytometry analyses of *T*-Memory cells (respectively gated $CD4^+/CD3^+$; and $CD8^+/CD3^+$; bar plots under green arrow) on $CD45RA^+CD62L^+$ (Tn), $CD45RA^-CD62L^+$ (Tcm), $CD45RA^-CD62L^-$ (Tem) and $CD45RA^+CD62L^-$ (Temra) subsets, in the IN compartments, in the presence or without co-treatment at 72 h. Data information: Data points are shown ± SEM. In the boxplots in (F), the centerline indicates the median, while the upper and lower lines represent the 75th and 25th percentiles, respectively. The whiskers represent the smallest and largest values in the 1.5 × interquartile range. Values on top indicate median. In (C, D), P values were calculated using unpaired Kruskal–Wallis test without multiple comparison correction. In (F) data were analyzed with unpaired Mann–Whitney test. $^*p < 0.05$, $^{**}p < 0.01$ compared to medium alone.

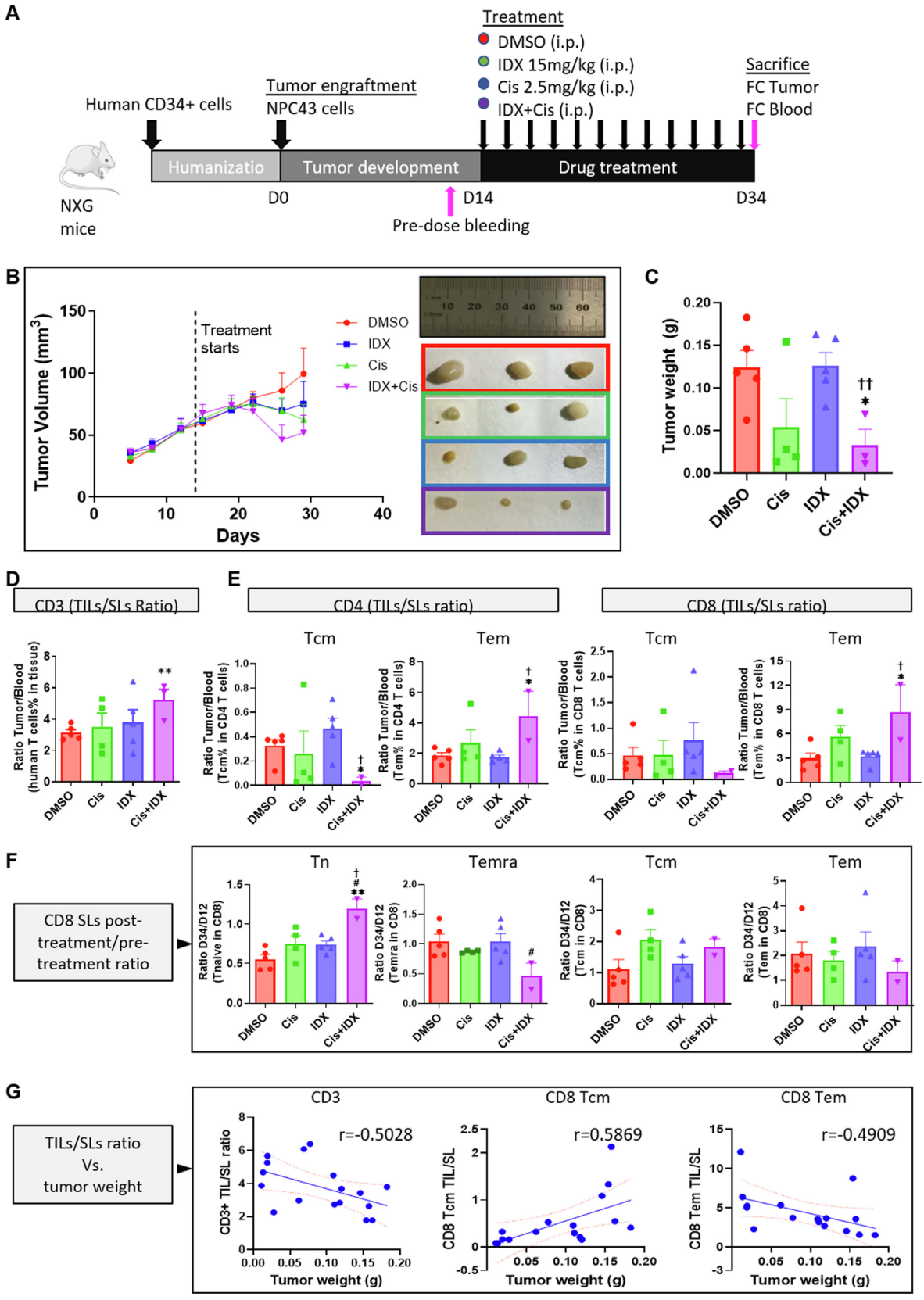
A
Treatment
DMSO (i.p.)
IDX 15mg/kg (i.p.)
Cis 2.5mg/kg (i.p.)
IDX+Cis (i.p.)
Sacrifice
FC Tumor
FC Blood
Human CD34+ cells
Tumor engraftment
NPC43 cells
Humanizatio
Tumor development
Drug treatment
NXG mice
D0
D14
D34
Pre-dose bleeding
B
Tumor Volume (mm3)
Treatment starts
DMSO
IDX
Cis
IDX+Cis
Days
C
Tumor weight (g)
DMSO
Cis
IDX
Cis+IDX
D
CD3 (TILs/SLs Ratio)
Ratio Tumor/Blood (human T cells% in tissue)
E
CD4 (TILs/SLs ratio)
CD8 (TILs/SLs ratio)
Tcm
Tem
Ratio Tumor/Blood (Tcm% in CD4 T cells)
Ratio Tumor/Blood (Tem% in CD4 T cells)
Ratio Tumor/Blood (Tcm% in CD8 T cells)
Ratio Tumor/Blood (Tem% in CD8 T cells)
F
CD8 SLs post-treatment/pre-treatment ratio
Tn
Temra
Ratio D34/D12 (Tnaive in CD8)
Ratio D34/D12 (Temra in CD8)
Ratio D34/D12 (Tcm in CD8)
Ratio D34/D12 (Tem in CD8)
G
TILs/SLs ratio Vs. tumor weight
CD3
CD8 Tcm
CD8 Tem
r=-0.5028
r=0.5869
r=-0.4909
CD3+ TIL/SL ratio
CD8 Tcm TIL/SL
CD8 Tem TIL/SL
Tumor weight (g)

[38]. Furthermore, our data suggest another potential interaction between tumor/immune cells upon combination treatment, whereby tumor cells are induced to generate higher TNFRSF1A levels that might directly interact with the TNFα produced by $CD8^+$ T cells. More importantly, the single-cell-derived gene signature also showed a significant association between TNFRSF1A-expressing malignant cells and TNFα-expressing $CD8^+$ T cells. This warrants further exploration to understand whether and how TNFSFR1A contributes to TNFα-dependent *T*-cell migration, activation and/or differentiation within the TME of NPC. Further studies aimed at understanding key regulators released from tumor cells upon combined treatment will also need to be considered.

The elevated $CD8^+$ Tem infiltration *in vitro* and in tumor spheroids upon combination therapy of IDX and Cis, translated into humanized mice, further supporting that the co-treatment could effectively reduce tumor growth *in vivo*. These findings are also supported by the public transcriptomic data, showing that memory *T*-cell populations are more likely to accumulate systemically as compared to paired tumor tissues. Given that Tem exhibits cytolytic effector functions whilst having limited access to the tumor site of NPC, this data favors a role for the co-treatment in promoting *T*-cell infiltration and modulating memory features with cytotoxicity. The clinical findings that NPC patients with high ENOX2 expression are associated with poorer prognosis, suggest that patients with high ENOX2-expressing tumors might have a more favorable response to the combined therapy. Thus, in addition to immune cell-mediated immunosurveillance, various factors, such as tumor-associated ENOX2 expression, likely alter the responsiveness of T cells and thereby treatment outcome. Precise and deeper understandings of the functional characteristics of ENOX2 will support the future development of effective treatments to patients who do not respond to chemotherapy. In those cases, co-treatment with an ENOX2 inhibitor could potentially elicit a durable tumor response.

Conclusion

In summary, the amount of $CD8^+$ T cells and tumor-associated ENOX2 expression within the TME are clearly different across cancer phenotypes. Building on this data, we speculate that NPC are amenable for successful treatment with the ENOX2 inhibitor, providing a rationale to further stratify patient tumors according to immune parameters. Notably, with respect to *T*-cell immunity, we provide evidence supporting the idea that combine current chemotherapy treatment with an ENOX2-targeted drug can drive immunologically- "cold" tumors into "hotter" phenotypes, via an elevated anti-tumor Tem cell population, that ultimately results in the sensitization of tumors to cytotoxic chemotherapy.

Funding

This work was funded by a Global Connections Fund Bridging Grant (Number 511490761) awarded by the Australian Academy of Technology and Engineering and Area of Excellent (AoE) Aoe/M−06/08 tissue bank. This work also received support from research funding of GRF 17122420; GRF 17114818; NSFC/RGC Joint research Scheme: 2018/19N_HKU735/18 and 81861168033. We also acknowledge the funding support from the Laboratory for Synthetic Chemistry and Chemical Biology under the Health@InnoHK Program launched by Innovation and Technology Commission, The Government of Hong Kong Special Administrative Region of the People's Republic of China.

Disclosures.

OL, XL and JW are Noxopharm Limited employees. Noxopharm Limited has a commercial interest in understanding the mechanisms of action of idronoxil, the active compound of its lead oncology drug Veyonda®. Other authors declare no potential conflicts of interest.

Compliance with Ethics Requirements

All procedure followed were in accordance with the ethical standards oh the responsible comitte on human experimentation (insitutional and national) and with the Helsinki Declaration of 1975,as revised in 2008 (5). Informed concent was obtained from all patients for being included in the study

All Insitutional and National Guidelines for the care use of animals (fisheries) were followed.

CRediT authorship contribution statement

Ngar-Woon Kam: Conceptualization, Investigation, Visualization, Writing – original draft, Writing – review & editing. **Olivier Laczka:** Conceptualization, Writing – review & editing. **Xiang Li:** Investigation, Writing – review & editing. **John Wilkinson:** Writing – review & editing. **Desmond Hung:** . **Syrus Pak Hei Lai:** Methodology. **Ka Chun Wu:** Methodology, Investigation. **Tsao Sai-Wa:** Supervision. **Wei Dai:** Visualization. **Che Chi Ming:** Supervision. **Victor Ho-Fun Lee:** Project administration, Supervision, Writing – review & editing. **Dora Lai-Wan Kwong:** Conceptualization, Funding acquisition, Project administration, Writing – review & editing.

Declaration of Competing Interest

The authors declare that they have no known competing financial interests or personal relationships that could have appeared to influence the work reported in this paper.

Fig. 6. *In vivo* efficacy of the combination therapy in humanized NPC mice model. (A) Schematic of combination treatment in NPC humanized mice model. IDX and Cisplatin were intraperitoneally injected 4 times a week at a dose of 15 mg/kg and 2.5 mg/kg respectively, in established NPC tumors of NXG mice. Blood and tumor were collected for flow cytometry (FC) analysis. **(B)** Excised tumor on day 34 of sacrifice (right) and tumor volume (left) change are shown in mice treated with vehicle (red), Cis (green), IDX (blue), or combination of both drugs (purple). **(C)** Tumor volume change is shown in mice treated with vehicle (red), Cis (green), IDX (blue), or combination of both drugs (purple). **(D)** Flow cytometry analysis on human *T*-cell enrichment (respectively gated CD3 +) in tumor tissue using frequency ratio of tumor infiltrating lymphocytes (TILs) to systemic lymphocytes (SLs), TILs/SLs. **(E)** Flow cytometry analysis on human CD4 + and CD8 + *T*-memory subsets (respectively gated CD4 + CD8- and CD4-CD8 + among CD3 +) enrichment in tumor tissue using frequency ratio of TILs/SLs. **(F)** Flow cytometry analysis on systemic changes of the differentiation in human CD8 + cells (respectively gated CD4-CD8 + among CD3 +) using frequency ratio of systemic lymphocytes (SLs) accumulated in blood on day 34 (post-treatment) compared to day 12 (pre-treatment), ratio D34/D12. **(G)** Correlation between tumor weight and ratio of TILs/SLs. Data information: Data points are shown ± SEM. In (C, D, E, F), data were analyzed with unpaired *t*-test. In (G), statistical evaluations were performed using Spearman's rank correlation test. *p < 0.05, **p < 0.01 compared to DMSO; #p < 0.05 compared to Cis; †p < 0.05 compared to IDX.

Acknowledgements

We thank Professor Maria Lung for kindly providing clinical materials and Dr Aya El Helali for her kind advice on the humanized mice model. We also thank Miss Lau Cho Yiu for her technical support. We also like to acknowledge the assistance of Imaging and Flow Cytometry Core of Centre for PanorOmic Sciences (CPOS).

Appendix A. Supplementary material

Supplementary data to this article can be found online at https://doi.org/10.1016/j.jare.2023.04.001.

References

[1] Chen YP, Chan ATC, Le QT, Blanchard P, Sun Y, Ma J. Nasopharyngeal carcinoma. Lancet 2019;394(10192):64–80.
[2] Wei WI, Sham JS. Nasopharyngeal carcinoma. Lancet 2005;365(9476):2041–54.
[3] Gong L, Kwong DL, Dai W, Wu P, Li S, Yan Q, et al. Comprehensive single-cell sequencing reveals the stromal dynamics and tumor-specific characteristics in the microenvironment of nasopharyngeal carcinoma. Nat Commun 2021;12(1):1540.
[4] Liu Y, He S, Wang XL, Peng W, Chen QY, Chi DM, et al. Tumour heterogeneity and intercellular networks of nasopharyngeal carcinoma at single cell resolution. Nat Commun 2021;12(1):741.
[5] Sallusto F, Geginat J, Lanzavecchia A. Central memory and effector memory T cell subsets: function, generation, and maintenance. Annu Rev Immunol 2004;22:745–63.
[6] Sallusto F, Lenig D, Forster R, Lipp M, Lanzavecchia A. Two subsets of memory T lymphocytes with distinct homing potentials and effector functions. Nature 1999;401(6754):708–12.
[7] Lanzavecchia A, Sallusto F. Regulation of T cell immunity by dendritic cells. Cell 2001;106(3):263–6.
[8] Mehlhop-Williams ER, Bevan MJ. Memory CD8+ T cells exhibit increased antigen threshold requirements for recall proliferation. J Exp Med 2014;211(2):345–56.
[9] Bindea G, Mlecnik B, Tosolini M, Kirilovsky A, Waldner M, Obenauf AC, et al. Spatiotemporal dynamics of intratumoral immune cells reveal the immune landscape in human cancer. Immunity 2013;39(4):782–95.
[10] Bruni D, Angell HK, Galon J. The immune contexture and Immunoscore in cancer prognosis and therapeutic efficacy. Nat Rev Cancer 2020;20(11):662–80.
[11] Aguero MF, Facchinetti MM, Sheleg Z, Senderowicz AM. Phenoxodiol, a novel isoflavone, induces G1 arrest by specific loss in cyclin-dependent kinase 2 activity by p53-independent induction of p21WAF1/CIP1. Cancer Res 2005;65(8):3364–73.
[12] Morre DJ, Chueh PJ, Yagiz K, Balicki A, Kim C, Morre DM. ECTO-NOX target for the anticancer isoflavene phenoxodiol. Oncol Res 2007;16(7):299–312.
[13] Alvero AB, Kelly M, Rossi P, Leiser A, Brown D, Rutherford T, et al. Anti-tumor activity of phenoxodiol: from bench to clinic. Future Oncol 2008;4(4):475–82.
[14] Herst PM, Davis JE, Neeson P, Berridge MV, Ritchie DS. The anti-cancer drug, phenoxodiol, kills primary myeloid and lymphoid leukemic blasts and rapidly proliferating T cells. Haematologica 2009;94(7):928–34.
[15] Georgaki S, Skopeliti M, Tsiatas M, Nicolaou KA, Ioannou K, Husband A, et al. Phenoxodiol, an anticancer isoflavene, induces immunomodulatory effects in vitro and in vivo. J Cell Mol Med 2009;13(9B):3929–38.
[16] Crumbaker M, Pathmanandavel S, Yam AO, Nguyen A, Ho B, Chan L, et al. Phase I/II Trial of the Combination of (177)Lutetium Prostate specific Membrane Antigen 617 and Idronoxil (NOX66) in Men with End-stage Metastatic Castration-resistant Prostate Cancer (LuPIN). Eur Urol Oncol 2021;4(6):963–70.
[17] Pathmanandavel S, Crumbaker M, Yam AO, Nguyen A, Rofe C, Hovey E, et al. (177)Lu-PSMA-617 and Idronoxil in Men with End-Stage Metastatic Castration-Resistant Prostate Cancer (LuPIN): Patient Outcomes and Predictors of Treatment Response in a Phase I/II Trial. J Nucl Med 2022;63(4):560–6.
[18] Kiknavelidze K, Shavdia M, Chikhladze N, Abshilava L, Messina M, Mautner G, et al. NOX66 as Monotherapy, and in Combination With Carboplatin, in Patients With Refractory Solid Tumors: Phase Ia/b Study. Curr Ther Res Clin Exp 2021;94:100631.
[19] Komada Y, Zhang SL, Zhou YW, Hanada M, Shibata T, Azuma E, et al. Cellular immunosuppression in children with acute lymphoblastic leukemia: effect of consolidation chemotherapy. Cancer Immunol Immunother 1992;35(4):271–6.
[20] Mackall CL, Fleisher TA, Brown MR, Magrath IT, Shad AT, Horowitz ME, et al. Lymphocyte depletion during treatment with intensive chemotherapy for cancer. Blood 1994;84(7):2221–8.
[21] Das RK, O'Connor RS, Grupp SA, Barrett DM. Lingering effects of chemotherapy on mature T cells impair proliferation. Blood Adv 2020;4(19):4653–64.
[22] Onyema OO, Decoster L, Njemini R, Forti LN, Bautmans I, De Waele M, et al. Chemotherapy-induced changes and immunosenescence of CD8+ T-cells in patients with breast cancer. Anticancer Res 2015;35(3):1481–9.
[23] Kam NW, Wu KC, Dai W, Wang Y, Yan LYC, Shakya R, et al. Peritumoral B cells drive proangiogenic responses in HMGB1-enriched esophageal squamous cell carcinoma. Angiogenesis 2021.
[24] Lanitis E, Dangaj D, Irving M, Coukos G. Mechanisms regulating T-cell infiltration and activity in solid tumors. Ann Oncol 2017;28(suppl_12):xii18-xii32..
[25] Chen DS, Mellman I. Elements of cancer immunity and the cancer-immune set point. Nature 2017;541(7637):321–30.
[26] Olson JA, McDonald-Hyman C, Jameson SC, Hamilton SE. Effector-like CD8(+) T cells in the memory population mediate potent protective immunity. Immunity 2013;38(6):1250–60.
[27] Klebanoff CA, Gattinoni L, Restifo NP. Sorting through subsets: which T-cell populations mediate highly effective adoptive immunotherapy? J Immunother 2012;35(9):651–60.
[28] Wherry EJ, Teichgraber V, Becker TC, Masopust D, Kaech SM, Antia R, et al. Lineage relationship and protective immunity of memory CD8 T cell subsets. Nat Immunol 2003;4(3):225–34.
[29] Kather JN, Halama N, Jaeger D. Genomics and emerging biomarkers for immunotherapy of colorectal cancer. Semin Cancer Biol 2018;52(Pt 2):189–97.
[30] Lin CY, Islam A, Su CJ, Tikhomirov AS, Shchekotikhin AE, Chuang SM, et al. Engagement with tNOX (ENOX2) to Inhibit SIRT1 and Activate p53-Dependent and -Independent Apoptotic Pathways by Novel 4,11-Diaminoanthra[2,3-b]furan-5,10-diones in Hepatocellular Carcinoma Cells. Cancers (Basel) 2019;11(3).
[31] Halama N, Michel S, Kloor M, Zoernig I, Benner A, Spille A, et al. Localization and density of immune cells in the invasive margin of human colorectal cancer liver metastases are prognostic for response to chemotherapy. Cancer Res 2011;71(17):5670–7.
[32] Martin MD, Kim MT, Shan Q, Sompallae R, Xue HH, Harty JT, et al. Phenotypic and Functional Alterations in Circulating Memory CD8 T Cells with Time after Primary Infection. PLoS Pathog 2015;11(10):e1005219.
[33] Darmon AJ, Pinkoski MJ, Bleackley RC. Granule-mediated cytotoxicity. Results Probl Cell Differ 1999;23:103–25.
[34] Pinkoski MJ, Waterhouse NJ, Heibein JA, Wolf BB, Kuwana T, Goldstein JC, et al. Granzyme B-mediated apoptosis proceeds predominantly through a Bcl-2-inhibitable mitochondrial pathway. J Biol Chem 2001;276(15):12060–7.
[35] Steinert EM, Schenkel JM, Fraser KA, Beura LK, Manlove LS, Igyarto BZ, et al. Quantifying Memory CD8 T Cells Reveals Regionalization of Immunosurveillance. Cell 2015;161(4):737–49.
[36] Doedens AL, Phan AT, Stradner MH, Fujimoto JK, Nguyen JV, Yang E, et al. Hypoxia-inducible factors enhance the effector responses of CD8(+) T cells to persistent antigen. Nat Immunol 2013;14(11):1173–82.
[37] Finlay DK, Rosenzweig E, Sinclair LV, Feijoo-Carnero C, Hukelmann JL, Rolf J, et al. PDK1 regulation of mTOR and hypoxia-inducible factor 1 integrate metabolism and migration of CD8+ T cells. J Exp Med 2012;209(13):2441–53.
[38] Palazon A, Tyrakis PA, Macias D, Velica P, Rundqvist H, Fitzpatrick S, et al. An HIF-1alpha/VEGF-A Axis in Cytotoxic T Cells Regulates Tumor Progression. Cancer Cell 2017;32(5):669–83 e5.